



AlignGemini: Generalizable AI-Generated Image Detection Through Task-Model Alignment

Ruoxin Chen¹ Jiahui Gao² Kaiqing Lin³ Keyue Zhang¹
Yandan Zhao¹ Isabel Guan⁴ Taiping Yao¹ Shouhong Ding¹

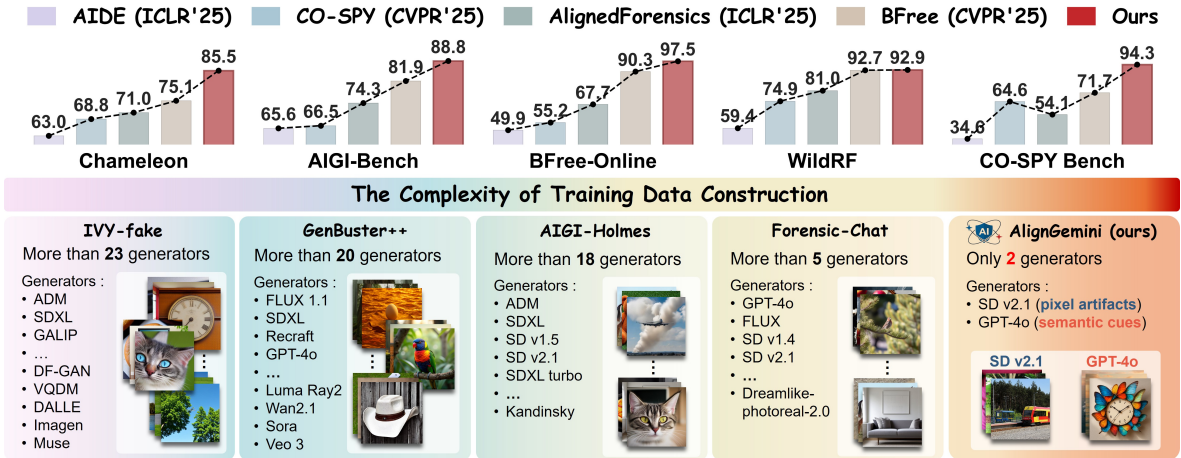


Figure 1. Top: Performance comparison on in-the-wild benchmarks. **AlignGemini consistently outperforms existing detectors across five datasets.** Bottom: Comparison on the complexity of training dataset construction. **AlignGemini relies on a substantially simpler training corpus.** Overall, AlignGemini achieves strong in-the-wild performance while significantly reducing training data complexity, supporting the effectiveness of Task-Model Alignment principle for AIGI detection.

Abstract

Vision Language Models (VLMs) are increasingly adopted for AI-generated images (AIGI) detection. However, while converting VLMs into detectors requires substantial resource, the resulting models often suffer from hallucination and poor generalization. To probe the core issue, we conduct an empirical analysis and reveal two characteristic behaviors: (i) fine-tuning VLMs with semantic supervision consistently strengthens semantic discrimination and generalizes well to unseen data; (ii) fine-tuning VLMs with pixel-artifact supervision leads to weak generalization. These observations indicate a fundamental task-model misalignment: **VLMs are inherently optimized for semantic reasoning and lack inductive bias toward low-level pixel artifacts, which lie outside their strengths.** Con-

versely, conventional vision models effectively capture low-level artifacts but exhibit insensitive to semantic inconsistencies compared to VLMs, highlighting that **different models are suited to different subtasks.** Motivated by this insight, we first formalize AIGI detection as two orthogonal subtasks—semantic consistency checking and pixel-artifact detection—and show that neglecting either induces systematic blind spots. We further propose the Task-Model Alignment principle and instantiate it in a two-branch detector, AlignGemini, which combines a VLM trained with pure semantic supervision and a pixel-artifact expert trained with pure artifact supervision. By enforcing pure supervision and orthogonal specialization, **each branch captures non-overlapping semantic or pixel cues, allowing AlignGemini to maximize complementary discrimination across the two dimensions.** Experiments on in-the-wild benchmarks show that AlignGemini improves average accuracy by **9.5%** with simplified training data. These results highlight task-model alignment as an effective principle for generalizable AIGI detection.

¹Tencent YouTu Lab ²East China University of Science and Technology ³Shenzhen University ⁴Hong Kong University of Science and Technology. Correspondence to: Ruoxin Chen <cusmochen@tencent.com>.

1. Introduction

The rapid progress of generative models (Goodfellow et al., 2014; Ho et al., 2020; Van Den Oord et al., 2016; Yan et al., 2025b) has fueled innovation across creative industries, but the growing volume of AI-generated images has heightened misinformation risks, making detection essential. Recently, VLMs have gained increasing attention, motivating their adaptation for AIGI detection. Early works (Xu et al., 2025a; Chen et al., 2024b) explore the potential of VLMs, and subsequent studies enhance VLM-based detectors via prompt engineering (Ji et al., 2025), reinforcement learning (Xu et al., 2025b; Zhou et al., 2025), curated datasets with fine-grained annotation (Xu et al., 2025b; Zhang et al., 2025; Kang et al., 2025; Wen et al., 2025b), reasoning-oriented mechanisms (Huang et al., 2025; Xia et al., 2025; Gao et al., 2025), and fusion with expert detectors (Chen et al., 2024b; Zhou et al., 2025; Peng et al., 2025; Tan et al., 2025).

However, recent studies show that VLMs face two fundamental limitations when adapted to AIGI detection (Gekhman et al., 2024; Lampinen et al., 2025; Yan et al., 2025a): (i) VLM detectors are prone to hallucinations, often producing incorrect labels with spurious explanations; (ii) explanation-oriented supervision is inherently ill-posed for synthetic images, which may be semantically faithful yet lack localized or describable visual artifacts, making artifact explanations ambiguous and unreliable. As a result, resource-intensive VLM-based approaches often fail to achieve robust generalization.

To investigate the core issue, we conduct an empirical analysis (Section 3) and identify **two characteristic behaviors**. (i) When fine-tuned with high-level semantic supervision, the VLM exhibits a substantial improvement in semantic discrimination and maintains strong generalization. (ii) In contrast, when fine-tuned on low-level pixel-artifact supervision, the VLM shows degraded generalization and frequent hallucinations. Conversely, conventional vision backbones achieve strong and stable performance in pixel-artifact detection. **These findings suggest that model performance is fundamentally governed by the alignment between task structure and the model’s inductive biases, which are shaped by its pretraining paradigm and architectural design.** When a model is forced to optimize objectives that are incongruent with its strength, this induces task–model misalignment and leads to suboptimal performance.

In this paper, we articulate a high-level design principle for AIGI detection through a series of coherent and systematic analyses, culminating in a detector that achieves strong in-the-wild performance: **1)** In Section 3, we show that AIGI detection inherently comprises two complementary subtasks: *semantic inconsistency detection* and *pixel-artifact detection*. Both are indispensable, as neglecting either subtask leads to systematic detection blind spots. **2)** We analyze

the behavior of different models on these two subtasks and reveal a clear division of inductive strengths, which forms the empirical foundation of the proposed *task–model alignment* principle. **3)** Guided by this, Section 4 introduces **AlignGemini**, which is trained using a substantially simplified training corpus. Without relying on complex annotations, reinforcement learning, or carefully-designed COT supervision, AlignGemini nevertheless achieves superior in-the-wild detection performance. Collectively, these results suggest **generalization in AIGI detection does not necessarily arise from scaling data volume or diversity, but rather from aligning training supervision with a model’s inherent inductive strengths.** Our contributions are:

- **A Principle-Level Framework for AIGI Detection.** We formulate **Task–Model Alignment** as a general design principle for AIGI detection by decomposing the task into two complementary subtasks: semantic inconsistency detection and pixel-artifact detection. Through controlled analysis, we show that different model families exhibit systematically different inductive strengths on these subtasks. Instantiating this principle, we introduce AlignGemini and demonstrate that aligning supervision with model inductive bias leads to strong in-the-wild generalization, even under substantially simplified training supervision.
- **An Evaluation Benchmark for Disentangled Detector Analysis.** We introduce **AIGI-Now**, a benchmark designed to support fine-grained evaluation of AIGI detectors. AIGI-Now spans nine contemporary image generators, including six commercial closed-source models, and provides two disjoint subsets per generator to disentangle semantic discrimination from pixel-artifact discrimination. This benchmark enables systematic analysis of detector behaviors beyond aggregate accuracy, facilitating principled diagnosis of generalization strengths and failure modes.

2. Related Works

AIGI Detection via Conventional Vision Models. CNNSpot (Wang et al., 2020) shows that a vanilla CNN readily detects synthetic images from *seen* generators but fails to generalize to *unseen* ones. UnivFD (Ojha et al., 2023) improves cross-generator generalization by adopting the VLM model CLIP as a backbone. Follow-up studies (Lin et al., 2025a; Tan et al., 2024a; Zheng et al., 2024; Yan et al.; Tan et al., 2024b; Chu et al., 2025; Li et al., 2024; Karageorgiou et al., 2025; Zhou et al., 2023; Tan et al., 2024c) pursue generalization by redesigning architectures, refining fine-tuning protocols, and tailoring loss functions. Nevertheless, these detectors predominantly rely on low-level pixel artifacts, making them brittle under post-processing.

AIGI Detection via VLM. VLMs excel at image-text semantic understanding, a capability that remains reliable

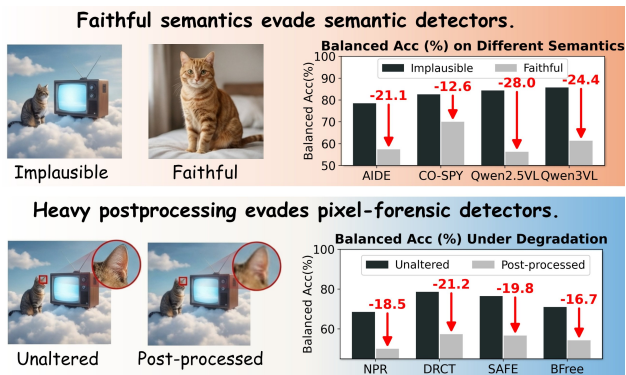


Figure 2. Illustration of systematic blind spots of semantic and pixel-artifact detectors. **Top:** semantically-faithful synthetic images evade semantic detectors despite clear pixel artifacts. **Bottom:** heavy degradations (e.g., compression, resizing) destroy the generation pixel trace, greatly reducing pixel-artifact detectors’ detection rate by 16%+, even for evidently implausible synthetic images.

under post-processing and helps distinguish semantically implausible fakes, making them attractive for AIGI detection. Early work UnivFD (Ojha et al., 2023) employs the VLM model CLIP (Radford et al., 2021) as a backbone to improve generalizability, followed by methods (Liu et al., 2024; Tan et al., 2024a) that further adapt CLIP for AIGI detection. With the emergence of large VLMs, later studies increasingly rely on scaling datasets and labels: FakeShield (Xu et al., 2025a) aggregates six datasets and, with GPT-4o-annotated defect regions and rationales; FakeVLM (Wen et al., 2025b) builds FakeClue dataset from five sources and employs three pretrained VLMs for aggregated annotation; IVY-Fake (Zhang et al., 2025), LEGION (Kang et al., 2025), BusterX++ (Wen et al., 2025a), Forensic-Chat (Lin et al., 2025b), VLM-Defake (Ji et al., 2025), and AIGI-Holmes (Li et al., 2025b) further expand coverage across generators, datasets, and forgery types via expert annotations or cross-LLM validation. **Overall, existing VLM-based detectors largely rely on large-scale datasets and high-fidelity supervision, incurring substantial annotation costs and introducing the risk of benchmark in-domaining, where overlapping or closely related generators appear in both training and evaluation, potentially overstating true generalization performance.** In contrast, *AlignGemini demonstrates that, under the Task-Model Alignment principle, large-scale training data and fine-grained annotation are not prerequisites for generalization.*

AIGI Detection via VLM with Experts. Extensive work (Cheng et al., 2025; Jia et al., 2024; Yoon et al., 2025; Grover et al., 2025) shows that VLMs are weak at pixel-level perception, and are therefore required for external experts. AIDE (Yan et al., 2024) couples CLIP with a shallow CNN to inject pixel-level cues. CO-SPY (Cheng et al., 2025) fuses CLIP semantic features with VAE reconstruction residuals to capture both semantic and pixel cues. Large VLMs (LVLMs) are adopted to strengthen the semantic

branch. X2-DFD (Chen et al., 2024b) augments the LVLm with expert detectors to recover pixel-level signals. AIGI-Holmes (Li et al., 2025b) pairs an LVLm with CLIP and NPR (Tan et al., 2024c) to integrate high- and low-level signals. AvatarShield (Xu et al., 2025b) similarly concatenates an additional residual-based expert module. In summary, external expert models are introduced to compensate for the inherent limitations of VLMs in low-level perception. However, in most existing approaches, these experts are incorporated in an ad hoc manner. Above methods separate semantics and pixels architecturally but overlook the most important, data dimension: their training sets remain mixed—some are semantically non-discriminative, others pixel-non-discriminative—entangling supervisory signals and limiting branch specialization. In contrast, *AlignGemini* jointly considers model inductive biases and supervision design. Specifically, the VLM is trained on a purely semantic corpus, while the expert model is trained on pixel-artifact cues. We show that this aligned pairing of model choice and task-pure supervision yields stronger branch specialization and leads to robust generalization.

3. Motivation

AIGI Detection as Two Sub-Tasks: Semantic and Pixel-Artifact Detection. AIGI detection decomposes into two complementary subtasks: (i) semantic-consistency verification, which assesses whether image content is semantically plausible, and (ii) pixel-artifact detection, which identifies low-level traces introduced by the generation process. Each subtask can succeed in isolation but exhibits systematic blind spots, as illustrated in Figure 2. Semantic detectors can be bypassed by content-faithful synthetic images, while pixel-based detectors are fragile under aggressive post-processing. *Each subtask captures a distinct failure mode, and reliance on either in isolation inevitably leaves systematic vulnerabilities.*

A Practical Analysis of Task-Model Alignment. Having established AIGI detection decoupled into two subtasks, we examine how different models align with these two subtasks. We construct three supervision regimes: (i) *Pixel-artifact set*: a pixel-artifact set, where synthetic images are generated via VAE reconstruction to preserve semantics while altering pixel statistics; (ii) *Semantically-implausible set*, where images contain semantic inconsistencies produced by GPT-4o and are aggressively post-processed to suppress low-level cues; (iii) a mixed set combining both. We train a VLM (Qwen-VL) and a conventional vision model (DINOv2) under each regime and observe the following (Figure 3). VLMs consistently excel at semantic-flaw detection, and semantic supervision further strengthens this capability with strong cross-generator generalization. However, they remain largely insensitive to pixel-level artifacts, even under explicit pixel supervision. In contrast,

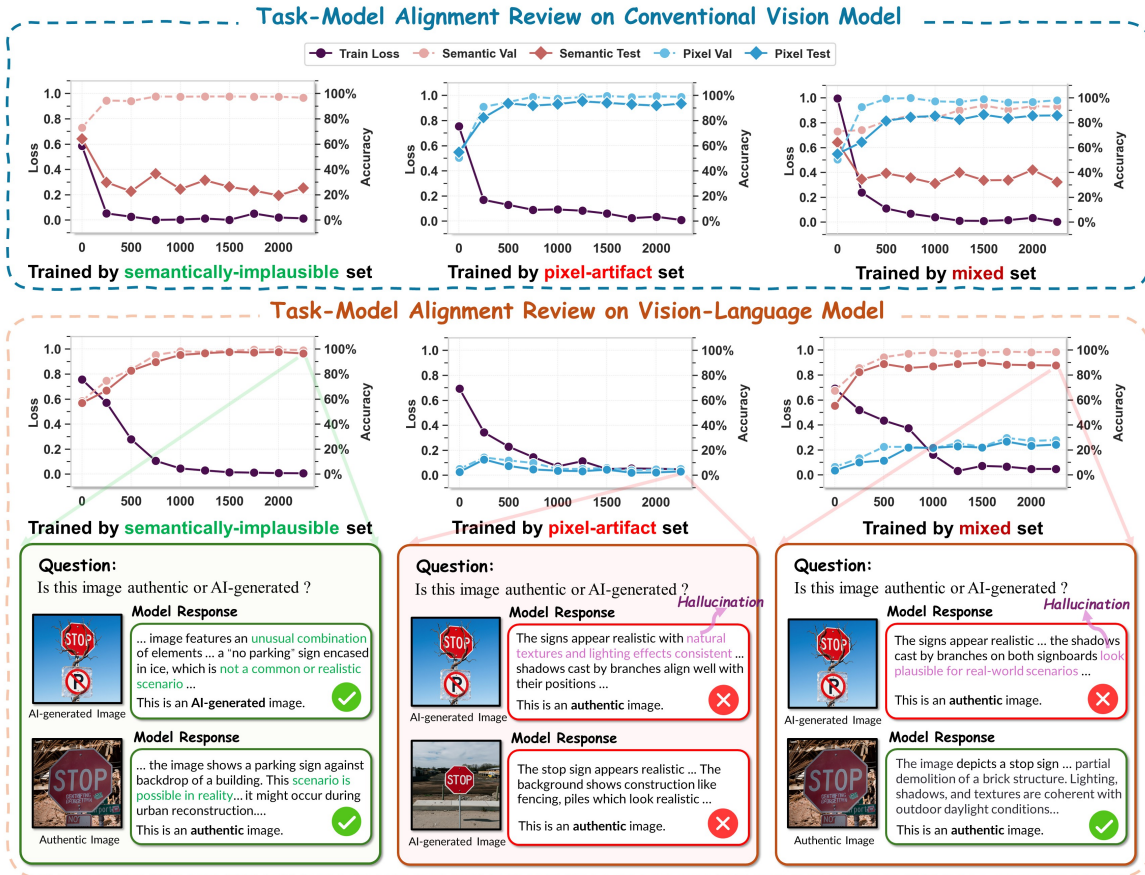


Figure 3. Analysis of task–model alignment. “Semantic/Pixel Val” denotes images generated by the same generator used in training. “Semantic/Pixel Test” denotes images from unseen generators. **Top:** DINOv2 trained with semantic supervision generalizes poorly to unseen semantic inconsistencies, whereas pixel-artifact supervision yields strong generalization on pixel-artifact tests. **Bottom:** Qwen-VL trained with semantic supervision robustly detects semantic flaws from unseen generators, while pixel-artifact supervision fails to improve its sensitivity to low-level artifacts. **Rightmost column:** Mixed semantic–pixel supervision degrades each model’s inherent strengths. **The results indicate that semantic and pixel subtasks align with different inductive biases. Joint supervision cannot reconcile this mismatch, whereas task–model alignment yields superior generalization.**

DINOv2 effectively captures pixel artifacts and generalizes well across generators, but performs poorly on semantic inconsistency detection. Notably, mixed semantic–pixel supervision fails to produce a single model that performs well on both subtasks, instead diluting each model’s strengths.

4. Methodology

Figure 4 shows the overall pipeline of our method. With only simplified data construction and lightweight fine-tuning, AlignGemini achieves remarkable in-the-wild detection.

Purity-First Orthogonal Dataset Construction for Task-Model Alignment. The dataset construction of AlignGemini emphasizes purity and orthogonality. As semantic inconsistencies are reliably captured by VLMs, the curation pipeline requires neither a VLM-as-judge nor human raters for label verification, mitigating label hallucination at its source. Accordingly, we construct two supervision sets in which semantic and pixel-artifact cues are disjoint by design. **(i) Semantical supervision set.** This set is used to

fine-tune the VLM and consists of 5,000 real images from Unsplash (Unsplash, 2025) and 5,000 semantically implausible synthetic images from Echo-4o (Ye et al., 2025).¹ To prevent leakage of low-level cues, both real and synthetic images undergo online randomized heavy post-processing during training, including resolution downsampling, JPEG compression, noise injection, and upsampling to the original size. This process perturbs pixel statistics, especially the downsampling–upsampling operation disrupts neighborhood pixel relationship. For annotation, we adopt a Direct Preference Optimization (DPO) protocol by prepending a fixed verdict prefix (“This is an AI-generated image.” / “This is an authentic image.”) and eliciting paired responses from Qwen2.5-VL-72B (Bai et al., 2025) to form preferred–dispreferred samples. **(ii) Pixel-artifact supervision set.** This set consists of natural images paired with their Stable Diffusion 2.1 VAE reconstructions, forming

¹Echo-4o (Ye et al., 2025) is an open-source collection of GPT-4o–conditioned surreal generations.

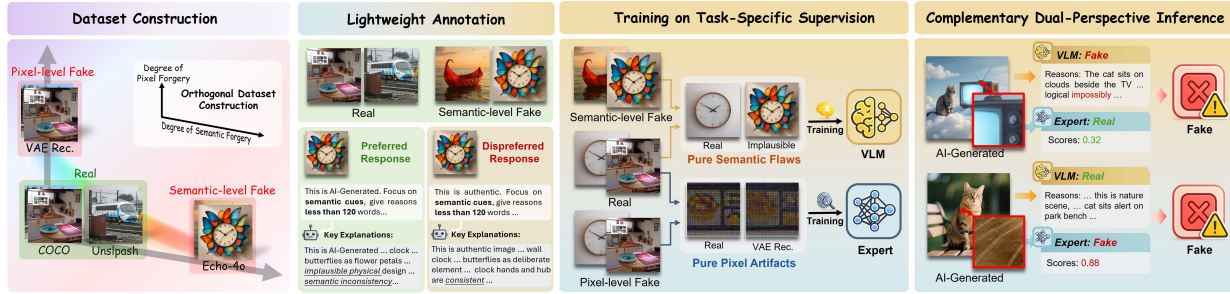


Figure 4. Illustration of the pipeline. **AlignGemini** adopts a deliberately simple yet effective design by constructing two orthogonal supervision sets. For semantic supervision, a pretrained VLM generates DPO-style labels explicitly constrained to semantic cues. The VLM and the expert are then fine-tuned separately, aligning each model with its corresponding subtask to encourage complementary specialization. At inference, **AlignGemini** jointly evaluates semantic and pixel-level cues, resulting in complementary AIGI detection.

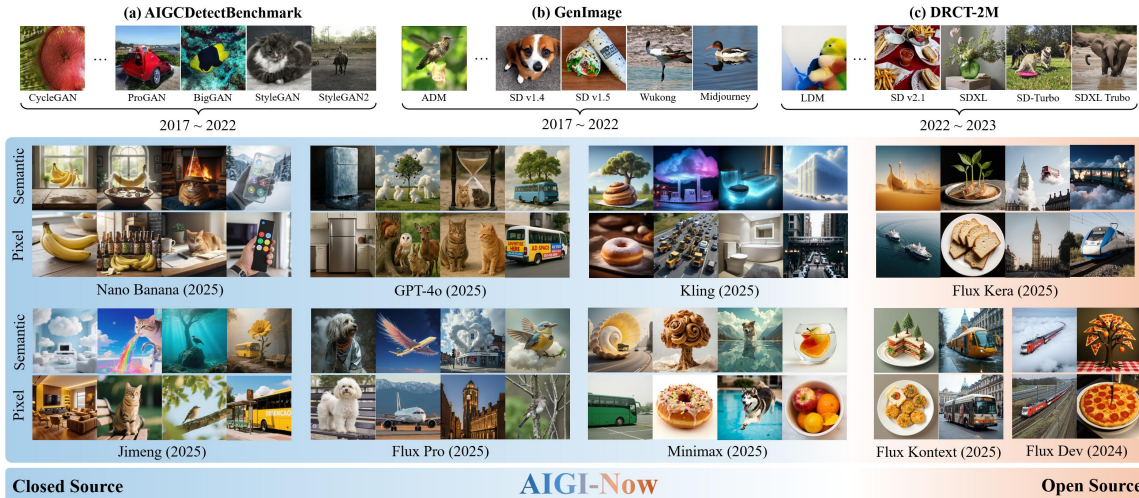


Figure 5. Comparison between **AIGI-Now** and existing benchmarks. **Top:** Existing benchmarks mainly rely on pre-2023 open-source generators. By contrast, real-world usage is dominated by newer commercial, closed-source models, creating a clear gap between the existing benchmark data and real-world fakes. **Bottom:** Our proposed **AIGI-Now** is constructed from the latest generators (all released after 2024), including six commercial, closed-source models such as GPT-4o with unknown architectures, enabling rigorous evaluation of detectors’ cross-architecture generalization and making the benchmark substantially closer to real-world application scenarios.

semantically matched pairs. This design removes semantic bias and isolates low-level discrepancies for pixel-artifact supervision. By keeping the two supervision sets orthogonal, **AlignGemini** allows each branch to specialize in its respective subtask, thereby improving the effectiveness of the integrated detector. Section 6 verifies that such orthogonality is critical for achieving robust generalization.

Training of AlignGemini. **AlignGemini** enforces task-model alignment by pairing each subtask with a model suited to its inductive strengths: a VLM (e.g., Qwen2.5-VL-7B (Bai et al., 2025)) for semantic discrimination and a vision expert (e.g., DINOv2) for pixel-forensic detection. The VLM branch is fine-tuned via Direct Preference Optimization (DPO) on the semantically implausible supervision, while the expert branch is fine-tuned on the pixel-artifact supervision using strictly low-level cues. This design preserves supervision orthogonality, prevents semantic leakage into the pixel expert, and maintains task-model alignment.

Inference of AlignGemini. At inference time, **AlignGemini** evaluates an input image using two complementary signals: semantic consistency and pixel-level artifact evidence. The underlying decision rule is conservative: since authentic images are expected to be benign along both dimensions, the presence of either semantic inconsistencies or pixel-level artifacts is sufficient to indicate synthesis. Accordingly, **AlignGemini** adopts a logical OR fusion, classifying an image as AI-generated if either the semantic or artifact branch produces a positive prediction. For semantically interpretable cues, the VLM branch provides linguistically grounded reasoning. In contrast, pixel-level artifacts, which are not readily expressible in natural language, are assessed via the expert model’s output logits.

5. Proposed Benchmark

AIGI-Now: A Diagnostic Benchmark for Disentangled Evaluation of AI-Generated Image Detection. As illustrated in Figure 5, **AIGI-Now** covers nine representative

Table 1. Overall comparison of balanced accuracy on five in-the-wild benchmarks.

Method	Chameleon	WildRF				AIGI-Bench			CO-SPY-Bench/in-the-wild					BFree-Online	Avg.	
		Facebook	Reddit	Twitter	Avg.	CommunityUI	SocialRF	Avg.	Civitai	DALL-E 3	instavibe.ai	Lexica	Midjourney-v6			Avg.
NPR _(CVPR24) (Tan et al., 2024c)	59.9	78.1	61.0	51.3	63.5	54.2	58.6	56.4	0.2	4.5	0.4	4.6	82.5	18.4	40.4	47.7 ± 16.6
UnivFD _(CVPR23) (Ojha et al., 2023)	50.7	49.1	60.2	56.5	55.3	51.4	54.6	53.0	3.0	10.3	0.3	1.2	20.8	7.1	48.8	43.0 ± 18.1
FatFormer _(CVPR24) (Liu et al., 2024)	51.2	54.1	68.1	54.4	58.9	51.9	55.4	53.7	0.0	1.7	0.0	2.8	32.2	7.3	50.0	44.2 ± 18.7
SAFE _(KDD25) (Li et al., 2024)	59.9	50.9	74.1	37.5	57.2	54.5	58.4	56.4	0.3	0.6	0.2	0.0	93.4	18.9	50.5	48.6 ± 15.2
C2P-CLIP _(AAAI25) (Tan et al., 2024a)	51.1	54.4	68.4	55.9	59.6	51.0	64.9	57.9	2.5	21.9	0.3	7.6	17.0	9.9	50.0	45.7 ± 18.3
AIDE _(ICLR25) (Yan et al., 2024)	65.8	57.8	71.5	48.8	59.4	66.2	64.9	65.6	15.1	33.1	6.9	26.6	91.3	34.6	49.9	60.2 ± 13.1
DRCT _(ICML24) (Chen et al., 2024a)	56.6	58.3	56.4	50.5	55.1	54.8	54.0	54.4	51.9	90.8	85.3	99.6	76.1	80.7	56.1	60.6 ± 10.1
AlignedForensics _(ICLR25) (Rajan et al., 2025)	71.0	91.6	70.9	80.6	81.0	75.6	73.0	74.3	97.8	68.0	8.0	0.5	96.4	54.1	67.7	69.6 ± 8.9
CO-SPY _(CVPR25) (Cheng et al., 2025)	68.8	72.2	77.7	74.8	74.9	65.2	67.7	66.5	96.3	69.0	37.6	68.8	51.4	64.6	55.2	66.0 ± 6.4
Forensic-Chat (Qwen2.5-VL)(Lin et al., 2025b)	-	77.8	83.4	82.1	81.1	74.6	89.8	82.2	-	-	-	-	-	-	-	-
BFree _(CVPR25) (Guillaro et al., 2024)	<u>75.1</u>	94.7	85.5	97.9	92.7	79.1	84.8	81.9	98.7	96.4	14.3	50.5	98.4	71.7	90.3	82.3 ± 9.2
AlignGemini	85.5	<u>92.2</u>	90.9	<u>95.5</u>	92.9	91.9	<u>85.6</u>	88.8	100.0	99.6	<u>75.0</u>	<u>96.8</u>	99.9	94.3	97.5	91.8 ± 4.7 (+9.5)

Table 2. Overall comparison of balanced accuracy on proposed AIGI-Now datasets.

Method	Nano Banana		GPT-4o		Jimeng		Kling		Minimax		Flux Pro		Flux Krea		Flux Dev		Flux Kontext		Avg.	
	Pix	Sem	Pix	Sem	Pix	Sem														
NPR _(CVPR24) (Tan et al., 2024c)	84.4	49.9	91.2	50.1	41.9	49.9	88.3	49.9	52.1	50.0	42.7	50.0	52.3	50.0	89.3	50.0	79.2	49.9	69.0 ± 21.2	50.0 ± 0.1
UnivFD _(CVPR23) (Ojha et al., 2023)	51.0	51.4	53.8	53.3	50.7	52.3	51.4	53.9	50.5	52.1	51.9	52.0	51.0	52.2	63.6	49.9	57.5	55.9	52.0 ± 2.3	52.6 ± 1.7
FatFormer _(CVPR24) (Liu et al., 2024)	53.4	49.9	49.9	49.8	48.4	49.9	54.8	50.0	49.1	50.0	48.4	50.0	49.5	50.0	52.4	50.0	63.6	49.9	52.1 ± 4.8	49.9 ± 0.1
SAFE _(KDD25) (Li et al., 2024)	99.3	50.1	99.7	50.4	50.0	50.5	99.6	50.0	49.8	50.1	49.9	50.5	51.2	50.1	99.8	<u>75.3</u>	98.8	83.4	77.5 ± 25.9	56.7 ± 13.0
C2P-CLIP _(AAAI25) (Tan et al., 2024a)	50.0	50.0	49.8	50.0	49.8	50.0	50.7	49.9	50.3	50.0	52.0	50.0	50.1	50.0	52.6	50.0	60.7	50.0	51.7 ± 3.5	50.0 ± 0.0
AIDE _(ICLR25) (Yan et al., 2024)	<u>98.9</u>	51.8	74.7	53.5	63.9	51.4	<u>98.2</u>	55.4	51.4	54.1	60.1	53.8	50.4	56.9	<u>99.1</u>	59.0	<u>97.9</u>	80.6	77.1 ± 21.4	57.4 ± 9.0
DRCT _(ICML24) (Chen et al., 2024a)	68.9	57.7	75.0	57.0	<u>89.3</u>	57.7	66.9	56.8	78.4	57.1	<u>83.0</u>	58.2	91.6	58.2	86.5	58.6	86.9	55.5	80.7 ± 8.9	57.4 ± 0.9
AlignedForensics _(ICLR25) (Rajan et al., 2025)	88.0	50.3	50.8	50.8	82.1	50.0	69.6	50.2	56.7	50.3	65.5	49.9	59.5	50.1	78.6	50.2	65.0	50.0	68.4 ± 12.4	50.2 ± 0.2
CO-SPY _(CVPR25) (Cheng et al., 2025)	74.1	<u>58.3</u>	78.9	<u>63.1</u>	83.0	<u>76.2</u>	88.3	<u>78.8</u>	<u>77.9</u>	65.6	77.3	<u>72.7</u>	<u>89.1</u>	74.0	88.5	74.9	65.1	66.0	80.2 ± 7.9	70.0 ± 6.9
BFree _(CVPR25) (Guillaro et al., 2024)	69.6	52.8	59.2	56.7	75.6	54.5	86.1	60.7	56.2	49.9	71.8	54.5	59.5	51.5	74.8	54.5	77.1	53.4	70.0 ± 9.9	54.3 ± 3.1
AlignGemini	96.0	95.6	<u>96.8</u>	95.7	96.2	95.6	<u>97.3</u>	94.9	91.3	89.8	89.9	93.2	83.0	92.6	96.6	95.3	86.6	88.0	92.6 ± 5.2 (+11.9)	93.4 ± 5.8 (+23.4)

Table 3. Overall comparison on three self-synthesized datasets.

Method	GenImage	DRCT-2M	AIGCDetectBenchmark	Avg.
NPR _(CVPR24) (Tan et al., 2024c)	51.5	37.3	53.1	47.3 ± 7.1
UnivFD _(CVPR23) (Ojha et al., 2023)	64.1	61.8	72.5	66.1 ± 4.6
FatFormer _(CVPR24) (Liu et al., 2024)	62.8	52.2	85.0	66.7 ± 13.7
SAFE _(KDD25) (Li et al., 2024)	50.3	59.3	50.3	53.3 ± 4.2
C2P-CLIP _(AAAI25) (Tan et al., 2024a)	74.4	59.2	81.4	71.7 ± 9.3
AIDE _(ICLR25) (Yan et al., 2024)	61.2	64.6	63.6	63.1 ± 1.4
DRCT _(ICML24) (Chen et al., 2024a)	84.7	90.5	81.4	85.5 ± 3.8
AlignedForensics _(ICLR25) (Rajan et al., 2025)	79.0	95.5	66.6	80.4 ± 11.8
CO-SPY _(CVPR25) (Cheng et al., 2025)	76.3	83.1	72.5	77.3 ± 5.4
BFree _(CVPR25) (Guillaro et al., 2024)	89.5	99.1	88.2	92.3 ± 6.0
AlignGemini	91.7	<u>98.1</u>	<u>87.7</u>	92.5 ± 5.2 (+0.2)

Table 4. Comparison with baseline methods under the same training set as AlignGemini, isolating the effect of data advantage.

Method	Chameleon	WildRF	AIGI-Bench	CO-SPY-Bench/in-the-wild	BFree-Online	Avg.
UnivFD	52.0	63.2	58.2	18.9	49.8	55.8 ± 17.3
AIDE	64.2	61.3	63.2	44.2	50.2	56.6 ± 8.9
CO-SPY	66.7	70.2	65.4	52.6	53.0	61.2 ± 8.0
NPR	58.3	56.9	54.2	12.3	48.9	46.1 ± 19.2
SAFE	61.2	62.4	55.3	21.7	52.6	50.6 ± 16.7
DINOv2-ViT-L-14	51.7	57.8	57.8	13.4	49.2	54.1 ± 18.6
Qwen2.5-VL-7B	65.7	86.3	80.4	67.6	82.9	76.6 ± 9.3
AlignGemini	85.5	92.9	88.8	94.3	97.5	91.8 ± 4.7 (+15.2)

image generators, including Nano Banana, GPT-4o, Jimeng, Kling, Minimax, Flux Pro, Flux Kera, Flux Kontext, and Flux Dev. For each generator, we sample 1,000 real images from the COCO test set (Lin et al., 2014) and extract their captions. Using both the original captions and deliberately constructed semantically perturbed variants, we synthesize paired images that are either semantically faithful or semantically implausible. Based on this controlled construction, AIGI-Now is organized into two complementary diagnostic subsets, explicitly disentangling semantic reasoning from low-level forensic evidence. The *semantic-discriminative* subset consists of real images and semantically implausible synthetic images, all subjected to aggressive post-processing to disrupt pixel-level statistics while preserving semantic inconsistency, thereby isolating semantic cues. In contrast, the *pixel-artifact-discriminative* subset includes real images and semantically faithful synthetic images, minimizing semantic shortcuts and emphasizing reliance on pixel-level forensic artifacts. More details are provided in Appendix.

6. Experiments

Experimental setup. We evaluate all methods on nine benchmarks, organized into three suites: (i) **five in-the-wild benchmarks**—Chameleon (Yan et al., 2024), WildRF (Cavia et al., 2024), AIGI-Bench (Li et al., 2025a), Co-SPY-Bench (in-the-wild) (Cheng et al., 2025), and

BFree-Online (Guillaro et al., 2024); (ii) **AIGI-Now**; and (iii) **three self-synthesized benchmarks**—GenImage (Zhu et al., 2023), DRCT-2M (Chen et al., 2024a), and AIGCDetectBenchmark (Zhong et al., 2024). Implementation details are provided in Appendix A.

Evaluation Metrics and Comparative Methods. Balanced accuracy is adopted as the primary metric, defined as the mean of the accuracies on real and synthetic images. The competitive methods include NPR (Tan et al., 2024c), FatFormer (Liu et al., 2024), UnivFD (Ojha et al., 2023), SAFE (Li et al., 2024), AIDE (Yan et al., 2024), C2P-CLIP (Tan et al., 2024a), DRCT (Chen et al., 2024a), AlignedForensics (Rajan et al., 2025), CO-SPY (Cheng et al., 2025), and BFree (Guillaro et al., 2024), Forensic-Chat (Lin et al., 2025b) ² All baselines are evaluated using their officially released checkpoints, without per-benchmark retuning. For AlignGemini, we consistently adopt a fine-tuned Qwen2.5-VL-7B as the VLM branch and a fine-tuned DINOv2 as the expert branch across all benchmarks. We organize our experiments around five key questions:

Q1. Does AlignGemini achieve stronger generalization?

²Other VLM-based detectors are excluded because (i) the training data overlap with some evaluation benchmarks, compromising fairness, or (ii) the pretrained weights are not publicly available.

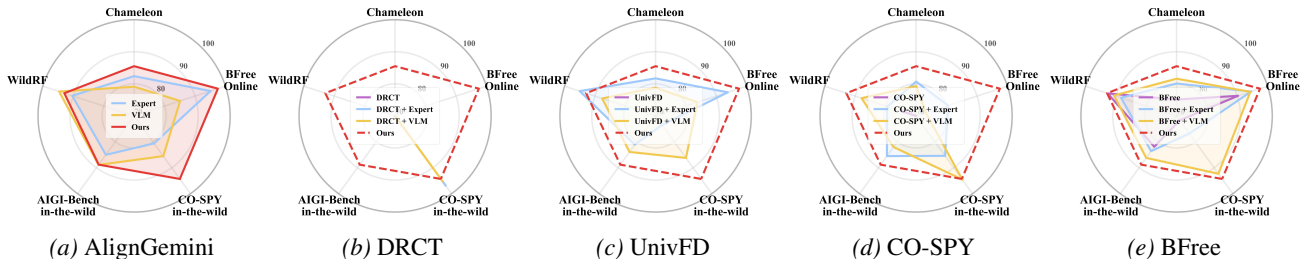


Figure 6. Ablation on the effect of using two models across five in-the-wild benchmarks. Each subfigure reports the in-the-wild performance of a baseline method augmented with one branch of AlignGemini, resulting in capacity-matched two-model-to-two-model comparisons. **AlignGemini consistently achieves non-trivial performance improvements, indicating that its gains are not solely attributable to the use of multiple models.**

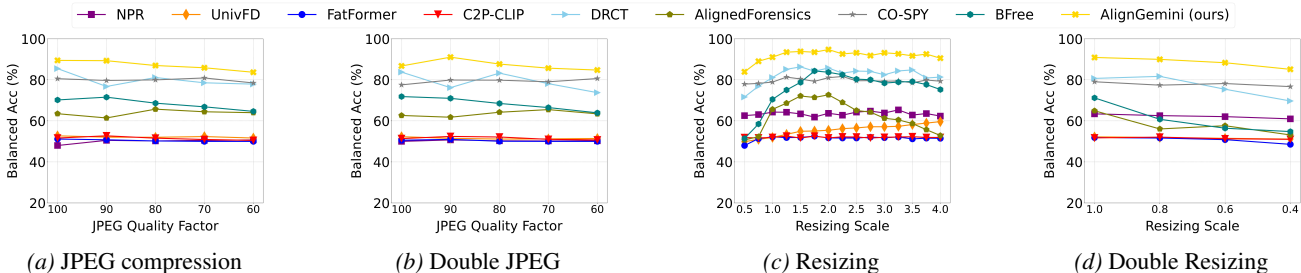


Figure 7. Robustness evaluation on AIGI-Now (pixel), which assesses robustness under common post-processing operations. Double JPEG compression applies the same JPEG quality factor twice in succession. Double resizing downsamples the image and then upsamples it back to the original resolution. Across all post-processing operations, AlignGemini consistently demonstrates superior robustness.

Comparison on Five In-The-Wild Benchmarks. Table 1 reports the performance on five in-the-wild benchmarks³. These benchmarks consist of Internet-sourced images generated by unknown models and processed with unknown pipelines, placing them out of distribution for all detectors and providing a faithful test of real-world generalization. In this challenging regime, most baselines achieve accuracies below 70, underscoring the difficulty. AlignGemini consistently surpasses all baselines, improving accuracy by **+9.5**, demonstrating its superior generalization.

Comparison on AIGI-Now and Three Self-Synthesized Benchmarks. Table 2 and Table 3 compare detectors on AIGI-Now, GenImage, DRCT-2M, and AIGCDetectBenchmark. Results on AIGI-Now reveal that most existing detectors exhibit limited pixel-level generalization to modern image generators: only DRCT and CO-SPY achieve balanced accuracies above 80%. In contrast, AlignGemini improves pixel-level accuracy by **+11.9**, demonstrating substantially stronger generalization. For semantic detection, nearly all baselines fail to identify semantic inconsistencies, yielding average accuracies below 70%, whereas AlignGemini achieves a markedly higher accuracy of **93.4**. AlignGemini also achieves the highest average accuracy across three self-synthesized benchmarks. Overall, these results indicate

³Results on CO-SPY-Bench/in-the-wild may differ from those reported in the original papers because the full in-the-wild set is not publicly available due to licensing restrictions; our evaluation is conducted on the subset provided by the CO-SPY authors.

that prior detectors are largely insensitive to semantic cues, while AlignGemini achieves strong generalization across both semantic and pixel-level subtasks.

Q2. Are AlignGemini’s performance gains attributable to task-model alignment, rather than the data advantages or the use of two models?

Ablation on Data Advantage. A natural concern is that our gains might arise from using more data. We therefore retrain all baselines on identical corpora comprising the same semantic and pixel-artifact supervision sets. As shown in Table 4, AlignGemini still yields a **+15.2** improvement. These supports *task-model alignment*: semantic-only supervision trains the VLM, and pure pixel-artifact supervision trains the expert. By contrast, forcing a single model to learn from mixed supervision dilutes both signals.

Ablation on the Effect of Using Two Models. Figure 6 presents a capacity-matched two-model-to-two-model comparison. Across all benchmarks, AlignGemini consistently outperforms augmented baseline methods, with its two-branch integration yielding improved accuracy on all five in-the-wild benchmarks. These results suggest that the observed gains are not attributable to merely employing multiple models—since augmenting baselines with either branch alone fails to achieve comparable performance—but **instead arise from principled task-model alignment, specifically orthogonal supervision and subtask specialization that promote effective complementarity.**

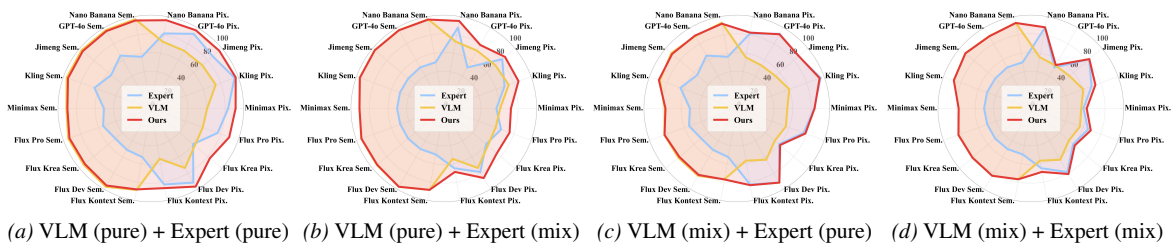


Figure 8. Performance on AIGI-Now under different supervision settings for the two branches. “Pure” denotes semantic-only supervision for the VLM branch and artifact-only supervision for the Expert branch, while “mix” applies combined semantic and pixel-level supervision. Pure supervision encourages stronger branch specialization and more effective complementarity, whereas mixed supervision dilutes specialization and results in degraded detection performance.

Table 5. Evaluate the in-the-wild accuracies and FLUX-specific accuracies of AlignGemini when upgrading the VLM backbone and the pixel experts. **SD/FLUX** denote experts trained on SD2/FLUX VAE-reconstructed images, respectively. **SD+FLUX** uses both experts jointly. The results show that performance consistently improves with stronger backbones and additional experts.

Method		In-the-wild benchmarks						AIGI-Now					
		Chameleon	WildRF	AIGI-Bench	CO-SPY-Bench/in-the-wild	BFree-Online	Avg.	Flux Pro.	Flux Kera.	Flux Dev	Flux Kontext.	Avg.	
Baseline	Qwen2.5-VL-7B (Untrained)	-	59.1	83.8	75.7	57.4	77.6	74.1 ± 11.8	69.6	67.7	73.3	66.9	69.4 ± 2.9
	CO-SPY	-	68.8	74.9	66.5	64.6	55.2	66.0 ± 6.4	75.0	81.5	81.7	65.6	75.9 ± 7.6
	BFree	-	75.1	92.7	81.9	71.7	90.3	82.3 ± 9.2	63.1	55.5	64.6	65.3	62.1 ± 4.5
AlignGemini	Qwen2.5-VL-7B	SD	85.5	92.9	88.8	94.3	97.5	91.8 ± 4.7 (+9.5)	91.5	87.7	95.9	87.3	90.6 ± 4.0 (+14.7)
	Qwen2.5-VL-7B	SD + FLUX	85.6	93.1	88.9	94.3	97.5	91.9 ± 4.7 (+9.6)	91.5	92.1	96.5	89.2	92.3 ± 3.1 (+16.4)
	Qwen3-VL-32B	SD	87.9	93.9	90.4	96.0	95.3	92.7 ± 3.4 (+10.4)	89.7	83.6	95.5	87.1	88.9 ± 5.0 (+13.0)
	Qwen3-VL-32B	SD + FLUX	88.4	94.4	90.8	96.3	95.6	93.1 ± 3.4 (+10.8)	89.8	90.5	96.4	89.1	91.4 ± 3.4 (+15.5)
	Qwen3-VL-235B	SD	89.8	94.0	91.2	97.2	97.8	94.0 ± 3.5 (+11.7)	93.1	89.9	97.0	87.8	92.0 ± 4.0 (+16.1)
	Qwen3-VL-235B	SD + FLUX	90.3	94.5	91.6	97.5	98.2	94.4 ± 3.5 (+12.1)	93.2	94.0	97.6	89.8	93.7 ± 3.2 (+17.8)

Q3. Does AlignGemini exhibit higher robustness?

Comparison on Robustness. Figure 7 evaluates robustness under four post-processing operations. Pixel-artifact-based detectors exhibit substantial performance degradation, particularly under double resizing with a scale factor of 0.4. In contrast, detectors that incorporate semantic features (e.g., CO-SPY) show improved stability. Notably, AlignGemini performs best across all evaluated settings.

Q4. How does task-specific supervision affect detection performance?

Ablation on Task-Specific Supervision. Figure 8 compares AlignGemini under task-pure supervision and mixed supervision. Results show that task-pure supervision consistently yields higher accuracy than mixed supervision. Mixed supervision dilutes branch-specific learning by encouraging each branch to model signals outside its inductive strengths, thereby weakening task specialization. In contrast, task-pure supervision enables stronger subtask specialization and more effective complementary behavior between branches, which is critical for improved generalization.

Q5. Is AlignGemini extensible?

Extensibility of AlignGemini. We emphasize that, our core contribution is a general design principle rather than a specific detector instantiation. Accordingly, AlignGemini is intentionally implemented as a lightweight proof of concept, with simplified data construction and fine-tuning strategies. Even under this constrained setting, AlignGemini exhibits improved generalization when scaled with stronger backbones or additional training data. As shown in Table 5,

we examine two complementary extension directions for AlignGemini. **VLM branch:** Scaling the backbone from Qwen2.5-VL-7B to Qwen3-VL-235B improves accuracy on Chameleon from 85.5 to 90.3, indicating that stronger VLM backbones offer an effective scaling path. **Expert branch:** Adding an additional expert trained on FLUX VAE reconstructions further enhances performance, particularly on FLUX-generated images. Overall, these results demonstrate that AlignGemini is readily extensible and that its performance scales naturally along both branches.

7. Conclusion

We propose the *Task-Model Alignment* principle to enhance the generalization of AI-generated image detection. Guided by this principle, we instantiate a practical framework, **AlignGemini**, demonstrating that even with simplified training corpora, effectively leveraging pretrained models’ inherent strengths can yield strong in-the-wild performance. Extensive experiments further validate the improved generalization, robustness, and extensibility of our approach. In addition, we release **AIGI-Now**, the first benchmark designed for disentangled evaluation of semantic and pixel-level discrimination capabilities.

8. Broader Impact

This work improves the generalization of AI-generated image detection, helping reduce risks associated with the misuse of generative models. In practice, our AlignGemini could be integrated into online platforms to assist in detecting AI-generated content and provide transparency to users, supporting more informed content consumption.

References

- Bai, S., Chen, K., Liu, X., Wang, J., Ge, W., Song, S., Dang, K., Wang, P., Wang, S., Tang, J., et al. Qwen2. 5-vl technical report. *arXiv preprint arXiv:2502.13923*, 2025.
- Cavia, B., Horwitz, E., Reiss, T., and Hoshen, Y. Real-time deepfake detection in the real-world. *arXiv preprint arXiv:2406.09398*, 2024.
- Chen, B., Zeng, J., Yang, J., and Yang, R. Drct: Diffusion reconstruction contrastive training towards universal detection of diffusion generated images. In *Forty-first International Conference on Machine Learning*, 2024a.
- Chen, Y., Yan, Z., Cheng, G., Zhao, K., Lyu, S., and Wu, B. X2-dfd: A framework for explainable and extendable deepfake detection. *arXiv preprint arXiv:2410.06126*, 2024b.
- Cheng, S., Lyu, L., Wang, Z., Zhang, X., and Schwag, V. Co-spy: Combining semantic and pixel features to detect synthetic images by ai. In *Proceedings of the Computer Vision and Pattern Recognition Conference*, pp. 13455–13465, 2025.
- Chu, B., Xu, X., Wang, X., Zhang, Y., You, W., and Zhou, L. Fire: Robust detection of diffusion-generated images via frequency-guided reconstruction error. In *CVPR*, 2025.
- Gao, Y., Chang, D., Yu, B., Qin, H., Chen, L., Liang, K., and Ma, Z. Fakereasoning: Towards generalizable forgery detection and reasoning. *arXiv preprint arXiv:2503.21210*, 2025.
- Gekhman, Z., Yona, G., Aharoni, R., Eyal, M., Feder, A., Reichart, R., and Herzig, J. Does fine-tuning llms on new knowledge encourage hallucinations? *arXiv preprint arXiv:2405.05904*, 2024.
- Goodfellow, I. J. et al. Generative adversarial nets. In *Advances in Neural Information Processing Systems*, 2014.
- Grover, R., Tamarapalli, J. S., Yerramilli, S., and Pande, N. Huemanity: Probing fine-grained visual perception in mllms. *arXiv preprint arXiv:2506.03194*, 2025.
- Guillaro, F., Zingarini, G., Usman, B., Sud, A., Cozzolino, D., and Verdoliva, L. A bias-free training paradigm for more general ai-generated image detection. *arXiv preprint arXiv:2412.17671*, 2024.
- Ho, J. et al. Denoising diffusion probabilistic models. *Advances in Neural Information Processing Systems*, 33: 6840–6851, 2020.
- Huang, T.-M., Lin, W.-T., Hua, K.-L., Cheng, W.-H., Yamagishi, J., and Chen, J.-C. Thinkfake: Reasoning in multimodal large language models for ai-generated image detection. *arXiv preprint arXiv:2509.19841*, 2025.
- Ji, Y., Hong, Y., Zhan, J., Chen, H., Zhu, H., Wang, W., Zhang, L., Zhang, J., et al. Towards explainable fake image detection with multi-modal large language models. *arXiv preprint arXiv:2504.14245*, 2025.
- Jia, S., Lyu, R., Zhao, K., Chen, Y., Yan, Z., Ju, Y., Hu, C., Li, X., Wu, B., and Lyu, S. Can chatgpt detect deepfakes? a study of using multimodal large language models for media forensics. In *Proceedings of the IEEE/CVF Conference on Computer Vision and Pattern Recognition*, pp. 4324–4333, 2024.
- Kang, H., Wen, S., Wen, Z., Ye, J., Li, W., Feng, P., Zhou, B., Wang, B., Lin, D., Zhang, L., et al. Legion: Learning to ground and explain for synthetic image detection. *arXiv preprint arXiv:2503.15264*, 2025.
- Karageorgiou, D., Papadopoulos, S., Kompatsiaris, I., and Gavves, E. Any-resolution ai-generated image detection by spectral learning. In *CVPR*, 2025.
- Lampinen, A. K., Chaudhry, A., Chan, S. C., Wild, C., Wan, D., Ku, A., Bornschein, J., Pascanu, R., Shanahan, M., and McClelland, J. L. On the generalization of language models from in-context learning and finetuning: a controlled study. *arXiv preprint arXiv:2505.00661*, 2025.
- Li, O., Cai, J., Hao, Y., Jiang, X., Hu, Y., and Feng, F. Improving synthetic image detection towards generalization: An image transformation perspective. *arXiv preprint arXiv:2408.06741*, 2024.
- Li, Z., Yan, J., He, Z., Zeng, K., Jiang, W., Xiong, L., and Fu, Z. Is artificial intelligence generated image detection a solved problem? *arXiv preprint arXiv:2505.12335*, 2025a.
- Li, Z., Yan, J., He, Z., et al. Is artificial intelligence generated image detection a solved problem? *arXiv preprint arXiv:2505.12335*, 2025b.
- Lin, K., Lin, Y., Li, W., Yao, T., and Li, B. Standing on the shoulders of giants: Reprogramming visual-language model for general deepfake detection. In *Proceedings of the AAAI Conference on Artificial Intelligence*, volume 39, pp. 5262–5270, 2025a.
- Lin, K., Yan, Z., Chen, R., Ye, J., Zhang, K.-Y., Zhou, Y., Jin, P., Li, B., Yao, T., and Ding, S. Seeing before reasoning: A unified framework for generalizable and explainable fake image detection. *arXiv preprint arXiv:2509.25502*, 2025b.
- Lin, T.-Y., Maire, M., Belongie, S., Hays, J., Perona, P., Ramanan, D., Dollár, P., and Zitnick, C. L. Microsoft coco: Common objects in context. In *European conference on computer vision*, pp. 740–755. Springer, 2014.

- Liu, H., Tan, Z., Tan, C., Wei, Y., Wang, J., and Zhao, Y. Forgery-aware adaptive transformer for generalizable synthetic image detection. In *Proceedings of the IEEE/CVF Conference on Computer Vision and Pattern Recognition*, pp. 10770–10780, 2024.
- Ojha, U. et al. Towards universal fake image detectors that generalize across generative models. In *Proceedings of the IEEE/CVF Conference on Computer Vision and Pattern Recognition*, pp. 24480–24489, 2023.
- Peng, S., Wang, Z., Gao, L., Zhu, X., Zhang, T., Liu, A., Zhang, H., and Lei, Z. Mllm-enhanced face forgery detection: A vision-language fusion solution. *arXiv preprint arXiv:2505.02013*, 2025.
- Radford, A. et al. Learning transferable visual models from natural language supervision. In *International Conference on Machine Learning*, pp. 8748–8763. PMLR, 2021.
- Rajan, A. S., Ojha, U., Schloesser, J., and Lee, Y. J. Aligned datasets improve detection of latent diffusion-generated images, 2025. URL <https://arxiv.org/abs/2410.11835>.
- Tan, C., Tao, R., Liu, H., Gu, G., Wu, B., Zhao, Y., and Wei, Y. C2p-clip: Injecting category common prompt in clip to enhance generalization in deepfake detection. In *Proceedings of the AAAI Conference on Artificial Intelligence*, 2024a.
- Tan, C., Zhao, Y., Wei, S., Gu, G., Liu, P., and Wei, Y. Frequency-aware deepfake detection: Improving generalizability through frequency space domain learning. In *Proceedings of the AAAI Conference on Artificial Intelligence*, volume 38, pp. 5052–5060, 2024b.
- Tan, C., Zhao, Y., Wei, S., Gu, G., Liu, P., and Wei, Y. Rethinking the up-sampling operations in cnn-based generative network for generalizable deepfake detection. In *Proceedings of the IEEE/CVF Conference on Computer Vision and Pattern Recognition*, pp. 28130–28139, 2024c.
- Tan, C., Wang, J., Ming, X., Tao, R., Wei, Y., Zhao, Y., and Lu, Y. Forenx: Towards explainable ai-generated image detection with multimodal large language models. *arXiv preprint arXiv:2508.01402*, 2025.
- Unsplash. Unsplash. <https://unsplash.com/data>, 2025.
- Van Den Oord, A., Kalchbrenner, N., and Kavukcuoglu, K. Pixel recurrent neural networks. In *International conference on machine learning*, pp. 1747–1756. PMLR, 2016.
- Wang, S.-Y. et al. Cnn-generated images are surprisingly easy to spot... for now. In *Proceedings of the IEEE/CVF Conference on Computer Vision and Pattern Recognition*, pp. 8695–8704, 2020.
- Wen, H., Li, T., Huang, Z., He, Y., and Cheng, G. Busterx++: Towards unified cross-modal ai-generated content detection and explanation with mllm. *arXiv preprint arXiv:2507.14632*, 2025a.
- Wen, S., Ye, J., Feng, P., Kang, H., Wen, Z., Chen, Y., Wu, J., Wu, W., He, C., and Li, W. Spot the fake: Large multimodal model-based synthetic image detection with artifact explanation. *arXiv preprint arXiv:2503.14905*, 2025b.
- Xia, C., Lin, M., Tan, J., Du, X., Qiu, Y., Zheng, J., Kong, X., Jiang, Y., and Zheng, B. Mirage: Towards ai-generated image detection in the wild. *arXiv preprint arXiv:2508.13223*, 2025.
- Xu, Z., Zhang, X., Li, R., Tang, Z., Huang, Q., and Zhang, J. Fakeshield: Explainable image forgery detection and localization via multi-modal large language models. In *The Thirteenth International Conference on Learning Representations*, 2025a.
- Xu, Z., Zhang, X., Zhou, X., and Zhang, J. Avatarshield: Visual reinforcement learning for human-centric video forgery detection. *arXiv preprint arXiv:2505.15173*, 2025b.
- Yan, H., Zheng, H., Wang, H., Yin, L., Liu, X., Cao, Z., Su, X., Chen, Z., Wu, J., Liao, M., et al. Visuriddles: Fine-grained perception is a primary bottleneck for multimodal large language models in abstract visual reasoning. *arXiv preprint arXiv:2506.02537*, 2025a.
- Yan, S., Li, O., Cai, J., Hao, Y., Jiang, X., Hu, Y., and Xie, W. A sanity check for ai-generated image detection. *arXiv preprint arXiv:2406.19435*, 2024.
- Yan, Z., Wang, J., Jin, P., Zhang, K.-Y., Liu, C., Chen, S., Yao, T., Ding, S., Wu, B., and Yuan, L. Orthogonal subspace decomposition for generalizable ai-generated image detection. In *Forty-second International Conference on Machine Learning*.
- Yan, Z., Lin, K., Li, Z., Ye, J., Han, H., Wang, Z., Liu, H., Lin, B., Li, H., Xu, X., et al. Can understanding and generation truly benefit together—or just coexist? *arXiv preprint arXiv:2509.09666*, 2025b.
- Ye, J., Jiang, D., Wang, Z., Zhu, L., Hu, Z., Huang, Z., He, J., Yan, Z., Yu, J., Li, H., et al. Echo-4o: Harnessing the power of gpt-4o synthetic images for improved image generation. *arXiv preprint arXiv:2508.09987*, 2025.
- Yoon, H., Jung, J., Kim, J., Choi, H., Shin, H., Lim, S., An, H., Kim, C., Han, J., Kim, D., et al. Visual representation

alignment for multimodal large language models. *arXiv preprint arXiv:2509.07979*, 2025.

Zhang, W., Jiang, C., Zhang, Z., Si, C., Yu, F., and Peng, W. Ivy-fake: A unified explainable framework and benchmark for image and video aigc detection. *arXiv preprint arXiv:2506.00979*, 2025.

Zheng, C., Lin, C., Zhao, Z., Wang, H., Guo, X., Liu, S., and Shen, C. Breaking semantic artifacts for generalized ai-generated image detection. *Advances in Neural Information Processing Systems*, 37:59570–59596, 2024.

Zhong, N., Xu, Y., Li, S., Qian, Z., and Zhang, X. Patchcraft: Exploring texture patch for efficient ai-generated image detection. *arXiv preprint arXiv:2311.12397*, pp. 1–18, 2024.

Zhou, Y., Fan, B., K. Atrey, P., and Ding, F. Exposing deepfakes using dual-channel network with multi-axis attention and frequency analysis. In *Proceedings of the 2023 ACM Workshop on Information Hiding and Multimedia Security*, pp. 169–174, 2023.

Zhou, Z., Luo, Y., Wu, Y., Sun, K., Ji, J., Yan, K., Ding, S., Sun, X., Wu, Y., and Ji, R. Aigi-holmes: Towards explainable and generalizable ai-generated image detection via multimodal large language models. *arXiv preprint arXiv:2507.02664*, 2025.

Zhu, M., Chen, H., Yan, Q., Huang, X., Lin, G., Li, W., Tu, Z., Hu, H., Hu, J., and Wang, Y. Genimage: A million-scale benchmark for detecting ai-generated image. *Advances in Neural Information Processing Systems*, 36: 77771–77782, 2023.

In this appendix, we provide additional technical and evaluative details:

- Section A presents implementation details and detailed comparison results on three self-synthesized benchmarks: GenImage, AIGCDetectBenchmark, and DRCT-2M.
- Section B compares the training and inference computational overhead of AlignGemini with other VLM-based detectors, highlighting the benefits of our simplified training corpus and lightweight system prompt.
- Section C describes the construction of our proposed AIGI-Now benchmark, including its data sources, generation protocol, and semantic/pixel-discriminative subsets.
- Section D visualizes AlignGemini’s outputs.

A. Implementation Details and Detailed Results of the Proposed AlignGemini

Implementation Details. (i) *VLM*: Qwen2.5-VL-7B (Bai et al., 2025) is used as the VLM backbone. During the DPO fine-tuning, we apply LoRA (rank =16, $\alpha=32$), using learning rate 1×10^{-6} , batch size 8, and DPO coefficient $\beta=0.05$ for one epoch. (ii) *Expert branch*: we adopt a DINOv2 backbone with a classification head, fine-tuned using LoRA (rank =8, $\alpha=1.0$) with learning rate 1×10^{-4} and batch size 16 on a pure pixel-artifact corpus constructed from VAE reconstructions: 11,8 k COCO training data paired with reconstructed counterparts. At inference, an image is classified as real only if both the VLM and the expert predict real; otherwise, it is synthetic.

Per-Benchmark Comparison Results. Beyond the results in Tables 3, we supplemented the detailed results of the individual subsets within each benchmark. These detailed results are reported in Tables 6–8. GenImage and DRCT-2M are dominated by diffusion-based images, while AIGCDetectBenchmark primarily consists of GAN-generated images. Comparisons of balanced accuracy on GenImage dataset are reported in Table 6. Following BFree (Guillaro et al., 2024), in order to align images’ format, we conduct JPEG-compression on synthetic images. Most methods suffer a significant decline when evaluated on these aligned images. Particularly, DRCT (Chen et al., 2024a) exhibits competitive performance on specific subsets such as Midjourney, SDv1.4, SDv1.5 and Wukong, but its performance degrades sharply on generators including ADM, GLIDE, and BigGAN. In contrast, our AlignGemini demonstrate better generalization across diverse generators, achieving an overall balanced accuracy of 91.7%. Comparisons of balanced accuracy on DRCT-2M dataset are reported in Table 7. AlignGemini achieves strong and stable performance across all DRCT-2M subsets, indicating robust generalization to a wide of diffusion generators. Specifically, our method consistently attains high balanced accuracy on both standard diffusion families and more challenging variants involving refinement, acceleration, and control mechanisms. Overall, AlignGemini reaches an average balanced accuracy of 98.1%. Across all benchmarks, AlignGemini achieves consistently strong performance and remains competitive with state-of-the-art methods. Notably, AlignGemini attains competitive performance on AIGCDetectBenchmark, despite not using any GAN-generated images during training. This result indicates strong cross-architecture generalization beyond the diffusion models seen during training.

Table 6. Comparison on GenImage. Following BFree (Guillaro et al., 2024), synthetic images are JPEG-compressed to match real images’ format.

Method	Midjourney	SDv1.4	SDv1.5	ADM	GLIDE	Wukong	VQDM	BigGAN	Avg.
NPR (CVPR 24) (Tan et al., 2024c)	53.4	55.1	55.0	43.8	41.2	57.4	48.4	57.7	51.5 ± 6.3
UnivFD (CVPR 23) (Ojha et al., 2023)	55.1	55.6	55.7	62.5	61.3	61.1	76.9	84.4	64.1 ± 10.8
FatFormer (CVPR 24) (Liu et al., 2024)	52.1	53.6	53.8	61.4	65.5	60.9	72.5	82.2	62.8 ± 10.4
SAFE (KDD 25) (Li et al., 2024)	49.0	49.7	49.8	49.5	53.0	50.3	50.2	50.9	50.3 ± 1.2
C2P-CLIP (AAAI 25) (Tan et al., 2024a)	56.6	77.5	76.9	71.6	73.5	79.4	73.7	85.9	74.4 ± 8.4
AIDE (ICLR 25) (Yan et al., 2024)	58.2	77.2	77.4	50.4	54.6	70.5	50.8	50.6	61.2 ± 11.9
DRCT (ICML 24) (Chen et al., 2024a)	82.4	88.3	88.2	76.9	86.1	87.9	85.4	87.0	84.7 ± 2.7
AlignedForensics (ICLR 25) (Rajan et al., 2025)	97.5	99.7	99.6	52.4	57.6	99.6	75.0	50.6	79.0 ± 22.7
CO-SPY (CVPR 25) (Cheng et al., 2025)	58.5	63.1	69.8	72.5	81.6	92.5	82.2	90.3	76.3 ± 11.4
BFree (CVPR 25) (Guillaro et al., 2024)	79.3	70.4	93.4	89.7	86.8	98.8	98.8	98.8	89.5 ± 9.3
AlignGemini	89.3	89.6	95.6	77.2	90.3	98.3	98.1	98.4	91.7 ± 7.5 (+2.2)

B. Overhead Comparison

Indirect Comparison of Overall Pipeline Overhead. A practical consideration for VLM-based detectors is the end-to-end pipeline overhead, including data construction, training, and inference. Table 9 reports indirect statistics for VLM-based detectors; because some official implementations are not publicly available, we compare them qualitatively rather than via unified wall-clock measurements⁴ The results highlight three advantages of AlignGemini-VLM: (i) its VLM branch

⁴The average tokens of IVY-FAKE and FakeVLM are obtained by referring to the IVY-FAKE (Zhang et al., 2025) paper.

Table 7. Comparison of balanced accuracy on DRCT-2M.

Method	LDM	SDv1.4	SDv1.5	SDv2	SDXL	SDXL-Refiner	SD-Turbo	SDXL-Turbo	LCM-SDv1.5	LCM-SDXL	SDv1-Ctrl	SDv2-Ctrl	SDXL-Ctrl	SDv1-DR	SDv2-DR	SDXL-DR	Avg.
NPR (CVPR24) (Tan et al., 2024c)	33.0	29.1	29.0	35.1	33.2	28.4	27.9	27.9	29.4	30.2	28.4	28.3	34.7	67.9	67.4	66.1	37.3 ± 15.0
UnivFD (CVPR23) (Ojha et al., 2023)	85.4	56.8	56.4	58.2	63.2	55.0	56.5	53.0	54.5	65.9	68.0	65.4	75.9	64.6	56.2	53.9	61.8 ± 8.9
FatFormer (CVPR24) (Liu et al., 2024)	55.9	48.2	48.2	48.2	48.2	48.3	48.2	48.2	48.3	50.6	49.7	49.9	59.8	66.3	60.6	56.0	52.2 ± 5.7
SAFE (KDD25) (Li et al., 2024)	50.3	50.1	50.0	50.0	49.9	50.1	50.0	50.0	50.1	50.0	49.9	50.0	54.7	98.2	98.5	97.3	59.3 ± 19.2
C2P-CLIP (AAAI25) (Tan et al., 2024a)	83.0	51.7	51.7	52.9	51.9	64.6	51.7	50.6	52.0	66.1	56.9	54.7	77.8	67.2	57.1	56.7	59.2 ± 9.9
AIDE (ICLR25) (Yan et al., 2024)	64.4	74.9	75.1	58.5	53.5	66.3	52.8	52.8	70.0	54.3	65.9	53.6	53.9	95.3	73.3	69.0	64.6 ± 11.8
DRCT (ICML24) (Chen et al., 2024a)	96.7	96.3	96.3	94.9	96.2	93.5	93.4	92.9	91.2	95.0	95.6	92.7	92.0	94.1	69.6	57.4	90.5 ± 7.4
AlignedForensics (ICLR25) (Rajan et al., 2025)	99.9	99.9	99.9	99.6	90.2	81.3	99.7	89.4	99.7	90.0	99.9	99.2	87.6	99.9	99.9	92.6	95.5 ± 6.1
CO-SPY (CVPR25) (Cheng et al., 2025)	72.2	99.4	82.4	99.3	73.7	96.7	70.9	92.2	94.8	51.0	51.5	99.4	99.4	50.7	83.9	91.1	83.1 ± 16.7
BFree (CVPR25) (Guillaro et al., 2024)	99.5	99.3	99.3	99.4	99.5	99.0	99.5	98.0	99.4	99.4	99.4	99.5	99.4	96.4	99.9	99.2	99.1 ± 0.8
Ours	99.1	98.7	98.8	98.2	98.0	98.9	97.7	94.6	96.4	98.3	98.6	99.0	99.2	98.9	99.2	96.2	98.1 ± 1.3 (-1.0)

Table 8. Comparison of balanced accuracy on AIGCDetectBenchmark.

Method	ADM	DALLE2	GLIDE	Midjourney	VQDM	BigGAN	CycleGAN	GauGAN	ProGAN	SDXL	SD14	SD15	StarGAN	StyleGAN	StyleGAN2	WFR	Wukong	Avg.
NPR (CVPR24) (Tan et al., 2024c)	43.8	20.0	41.2	53.4	48.4	53.1	76.6	42.2	58.7	59.6	55.1	55.0	67.4	57.9	54.6	58.8	57.4	53.1 ± 12.2
UnivFD (CVPR23) (Ojha et al., 2023)	62.5	50.0	61.3	55.1	76.9	87.5	96.9	98.8	99.4	58.2	55.6	55.7	95.1	80.0	69.4	69.2	61.1	72.5 ± 17.3
FatFormer (CVPR24) (Liu et al., 2024)	80.2	68.5	91.1	54.4	88.0	99.2	99.5	99.1	98.5	71.7	67.5	67.2	92.4	98.0	98.8	88.3	75.6	85.0 ± 14.9
SAFE (KDD25) (Li et al., 2024)	49.5	49.5	53.0	49.0	50.2	52.2	51.9	50.0	50.0	49.8	49.7	49.8	50.1	50.0	50.0	49.8	50.3	50.3 ± 1.1
C2P-CLIP (AAAI25) (Tan et al., 2024a)	71.6	52.3	73.5	56.6	73.7	98.4	96.8	98.8	99.3	62.3	77.5	76.9	99.6	93.1	79.4	94.8	79.4	81.4 ± 15.6
AIDE (ICLR25) (Yan et al., 2024)	52.9	51.1	60.2	49.8	69.3	70.1	93.6	60.6	89.0	49.6	51.6	51.0	72.1	66.5	59.0	80.6	54.5	63.6 ± 13.9
DRCT (ICML24) (Chen et al., 2024a)	79.9	89.2	89.2	85.5	88.6	81.4	91.0	93.8	71.1	88.3	91.4	91.0	53.0	62.7	63.8	73.9	90.8	81.4 ± 12.2
AlignedForensics (ICLR25) (Rajan et al., 2025)	51.6	52.0	55.6	96.2	72.1	51.2	49.5	50.8	50.7	95.1	99.7	99.6	53.8	52.7	51.6	50.0	99.6	66.6 ± 21.6
CO-SPY (CVPR25) (Cheng et al., 2025)	58.5	84.9	81.7	69.8	72.6	70.5	53.5	68.1	74.0	81.4	92.5	92.2	62.8	60.0	60.1	60.9	90.2	72.5 ± 12.6
BFree (CVPR25) (Guillaro et al., 2024)	79.3	85.8	86.8	93.4	89.7	91.9	76.8	97.0	95.9	99.3	98.8	98.8	86.1	82.1	78.0	60.5	98.8	88.2 ± 10.5
AlignGemini	89.3	94.9	90.3	95.6	77.2	90.4	74.4	92.5	91.0	99.1	98.3	98.1	72.9	86.6	89.2	52.6	98.4	87.7 ± 12.2 (-0.5)

is trained with fewer samples than competing VLM-based detectors, reducing training overhead; (ii) it does not require manual annotation checking, since semantically implausible images can be reliably labeled by the model itself; and (iii) it adopts a concise system prompt that forces the VLM to focus exclusively on identifying semantic flaws, while delegating the pixel-artifact detection task—which is particularly difficult for VLMs and prone to hallucinations—to a dedicated expert model. As a result, the VLM branch exploits its inherent semantic perception capabilities to detect high-level semantic inconsistencies “at a glance”. Moreover, the overhead of AlignGemini’s expert branch, which mainly consists of VAE reconstruction and LoRA fine-tuning of DINOv2, is negligible compared with that of the VLM branch.

Table 9. Comparison of training data and inference cost for VLM-based detectors.

Method	Backbone	Training			Inference		
		Training samples	Annotation type	Annotation check	Avg. tokens ↓	Sec. / token	Sec. / Ans. ↓
IVY-FAKE (Zhang et al., 2025)	Ivy-VL-LLaVA	150K	Automated by Gemini 2.5 pro	LLM	530	0.0424	22.47
FakeVLM (Wen et al., 2025b)	LLaVA-v1.5-7B	95K	Automated by 3 MLLMs	LLM	120	0.0128	1.54
AIGI-Holmes (Li et al., 2025b)	LLaVA-v1.6-Mistral-7B	69K	Automated by 4 MLLMs	LLM + Human	181	0.0057	1.03
Forensics-Chat (Lin et al., 2025b)	Qwen2.5-VL-7B	61K	Automated by Gemini 2.5 pro	None	307	0.0062	1.90
AlignGemini-VLM	Qwen2.5-VL-7B	10K	Automated by Qwen2.5-VL-7B	None	97	0.0062	0.60

C. Design of the AIGI-Now Benchmark

Overview of Employed Generative Models. AIGI-Now covers widely used modern generators, including nine generative models:

- Nano Banana⁵ (Google Gemini 2.5 Flash Image): a state-of-the-art commercial image generation and editing model from Google Gemini.
- GPT-4o⁶: OpenAI’s integrated text-to-image model with strong prompt adherence and text rendering.
- Jimeng⁷ (jimeng-t2i-v30): a multimodal commercial model from ByteDance supporting high-quality text-to-image generation.
- Kling⁸ (kling-v2): a commercial model developed by Kuaishou for high-quality image and video generation.
- Minimax⁹ (image-01): MiniMax’s flagship text-to-image model optimized for realistic, prompt-faithful imagery.

⁵<https://deepmind.google/models/gemini/image/>

⁶<https://openai.com/index/introducing-4o-image-generation/>

⁷<https://jimeng.jianying.com/>

⁸<https://app.klingai.com/>

⁹<https://minimaxi.com/>

- Flux Pro¹⁰ (flux1.1-pro): a text-to-image model from Black Forest Labs combining high visual quality with fast inference.
- Flux Dev¹¹: a general-purpose FLUX.1 model for high-quality text-to-image generation.
- Flux Krea¹²: a FLUX.1 variant tailored for creative and stylized image generation.
- Flux Kontext¹³: a FLUX.1 model for image generation and editing that can preserve contextual details and text–image consistency.

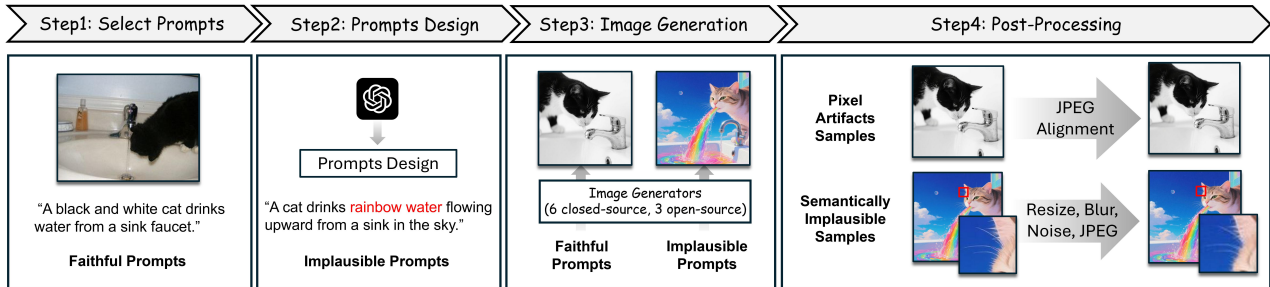


Figure 9. Overall pipeline for constructing the AIGI-Now benchmark.

Overall Pipeline of Constructing AIGI-Now. Figure 9 illustrates the overall pipeline for constructing AIGI-Now. For each generative model, the construction proceeds in four stages: (i) we randomly sample real images from the COCO test split; (ii) starting from the associated captions, we construct two types of prompts, namely semantically faithful prompts (for pixel-artifact subsets) and semantically implausible prompts (for semantic subsets), as described above; (iii) we employ generative model to synthesize images conditioned on these prompts; and (iv) we form pixel-artifact and semantic subsets with targeted pre- and post-processing. For the pixel-artifact subsets, which consist of real images and semantically faithful synthetic images, we align the formats of synthetic samples with their real counterparts by applying the same JPEG compression settings, thereby mitigating format bias. For the semantic subsets, which consist of real images and semantically implausible synthetic images, we apply a suite of heavy post-processing operations to both real and synthetic images to prevent detectors from exploiting low-level artifacts. Specifically, each image undergoes the following operations: (i) it is first downsampled to 40% of its original resolution; (ii) Gaussian noise with a standard deviation of 0.1 is injected; (iii) a Gaussian blur with a radius of 0.20 is applied; (iv) the image is re-encoded using JPEG compression with a quality factor of 80; and (v) the degraded image is upsampled back to its original resolution. These transformations substantially distort low-level statistics while preserving high-level semantics, forcing detectors to rely on robust forensic cues rather than brittle artifacts.

Prompt Design. AIGI-Now uses the widely adopted COCO dataset as the source of real images. Starting from COCO captions, we design two types of prompts. (i) *Semantically faithful* prompts, used to construct pixel-artifact subsets: we directly adopt the original COCO captions to synthesize images whose semantic content roughly matches the corresponding real images. (ii) *Semantically implausible* prompts, used to construct semantic subsets: we leverage LLM to inject physically impossible, surreal, or logically contradictory attributes into the original COCO captions while preserving the main entities. Representative examples of semantically implausible prompts are shown in the prompt box in Figure 10.

Visualization of the AIGI-Now Benchmark. Figures 11 and 12 illustrate the semantic and pixel-artifact subsets of AIGI-Now, spanning nine different generative models. These examples provide an intuitive view of high-quality synthetic images produced by recent generative models and highlight the challenges they pose to AIGI detectors.

¹⁰<https://bfl.ai/models/flux-pro>

¹¹<https://huggingface.co/black-forest-labs/FLUX.1-dev>

¹²<https://huggingface.co/black-forest-labs/FLUX.1-Krea-dev>

¹³<https://huggingface.co/black-forest-labs/FLUX.1-Kontext-dev>

Semantically Implausible Prompts

1. A woman sitting at a table in front of a pile of *glowing* luggage.
 2. A pile of *melting* luggage in a room with two women nearby.
 3. The man stands holding a surfboard as he looks out at a *sea of stars*.
 4. A couple celebrating a birthday in a kitchen *underwater*.
 5. Lots of skiers standing atop a hill of *giant crystals*.
 6. Skiers and snowboarders standing on a mountain of *giant clocks*.
 7. a young boy standing in front of a ball *made of stars*.
 8. A man with fruit *made of glass* on the back of a pickup truck.
 9. A group of skiers gather on a hill *made of clouds*.
 10. A man holding a *clock-shaped* object in his hand.
 11. A man playing tennis on *clouds*.
 12. A living room with a *floating* TV and a *glowing* wheel.
 13. A bathroom overlooking an *upside-down* ocean.
 14. A city intersection where traffic lights *rain upward*.
 15. A horse in a snowy pasture with a *neon-lit* fence.
 16. Man at market with *glowing blue* bananas.
 17. A boy jumping on a skateboard with *wings*.
 18. A farmer’s market filled with *giant* bananas and *shadowless* people.
 19. A group beside a *glowing* bench with *transparent* frisbees.
 20. Breakfast and juice served *on a cloud*.
 21. A bench on a beach *on the moon*.
 22. An empty street with *floating* buildings and *upside-down* cars.
 23. A black and white image of an old person *melting into shadows*.
 24. A city intersection sign made of *ice* in front of a building of *clouds*.
 25. A bus stopped on the side of a road that *melts into a river*.
 26. A white dog made of *clouds* standing on a *floating* wooden bench.
 27. Stop sign with a tree branch made of *liquid metal* touching it.
 28. A man sitting on a bench with an ocean of *liquid glass* behind him.
 29. A giant clock on the very top of a building *growing like a tree*.
 30. A kitchen with a *glowing* refrigerator and *floating* counter chairs.
 31. A bunch of bikes with *wings* lined up on a *cloud* curb.
 32. A highway made of *glass* filled with traffic and *golden* buses.
-

Figure 10. Illustrative prompts used in AIGI-Now.



(a) Flux-kera



(b) Flux-Kontext



(c) Flux-Dev

Figure 11. Representative AIGI-Now examples synthesized by Flux-Kera, Flux-Kontext, and Flux-Dev, illustrating the high visual fidelity and stylistic diversity of recent Flux generators.

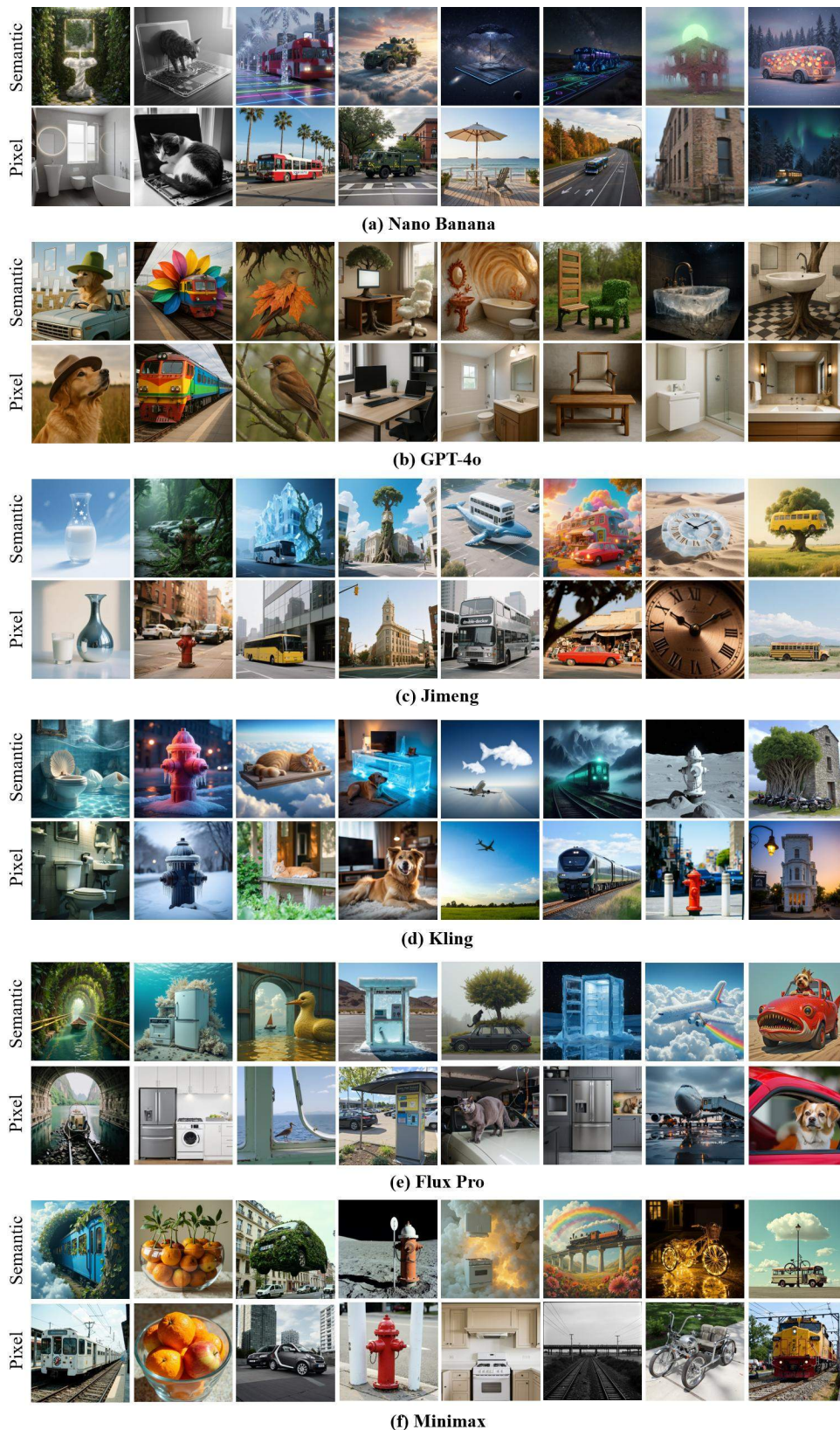


Figure 12. Representative AIGI-Now examples generated by six recent closed-source models, showcasing diverse scenes and styles that increase the difficulty of robust AI-generated image detection.

D. Visualization of AlignGemini Outputs

System Prompt of AlignGemini’s VLM. Figure 13 illustrates the system prompt used for AlignGemini’s VLM detector. Unlike prior VLM detectors (e.g., AIGI-Holmes), whose system prompts exhaustively enumerate possible visual artifacts and require the model to check them one by one, our prompt explicitly instructs the VLM to (i) focus strictly on semantic and logical reasoning and (ii) provide concise, evidence-based rationales in fewer than 120 words. This design steers the model toward detecting semantic inconsistencies rather than low-level pixel artifacts, reduces inference cost by generating substantially fewer tokens, and alleviates hallucinations by deliberately avoiding instructions to attend to fine-grained visual artifacts.

System Prompt

Role: AI visual assistant.

You are an AI visual assistant that analyzes a single image to determine whether it is authentic or AI-generated.

Tasks

1. <rationale> section:
 - Provide concise, evidence-based reasoning in fewer than 120 words.
 - Focus strictly on semantic or logical reasoning.
2. <answer> section:
 - If real: only output “This is an authentic image.”
 - If AI-generated: only output “This is an AI-generated image.”

Output Structure (must match exactly):

<rationale></rationale>

<answer></answer>

Figure 13. System prompt.

AlignGemini preserves general capabilities of the VLM. Table 10 quantitatively compares different VLM-based detectors in terms of their general multimodal understanding capabilities. The results show that AlignGemini preserves substantially more of the VLM’s general capabilities than other detectors, mainly due to two factors: (i) our training strategy that reinforces the VLM’s inherent strengths and (ii) preference-guided DPO fine-tuning. Specifically, AlignGemini does not force the VLM to learn misaligned skills such as explicit pixel-artifact identification, and it avoids supervised fine-tuning on curated “hard” samples that typically damage general multimodal understanding. Figure 14 provides qualitative visual examples. These examples show that, despite being adapted for AIGI detection, the VLM still preserves strong general multimodal capabilities, because our training strategy maintains its inherent strengths rather than pushing it to learn tasks misaligned with those strengths.

Table 10. Comparison of AlignGemini and baseline VLM-based detectors on general multimodal understanding benchmarks. Results are referred from (Lin et al., 2025b).

Method	BLINK	RealWorldVQA	MME	MMT-Bench _{VAL}
General MLLM				
Qwen-2.5-VL-3B	0.4750	0.6588	1590	0.6025
Qwen-2.5-VL-7B	0.5481	0.6758	1677	0.5948
LLaVA-1.5-7B	0.4171	0.5424	1436	0.4713
MLLM-based AIGI detector				
FakeVLM	0.3761	0.5385	1221	0.4445
Forensic-Chat	0.5139	0.6745	1625	0.5849
AlignGemini	0.5321	0.6759	1643	0.5911

Visualization of AlignGemini’s outputs. Figures 15–20 present qualitative examples of AlignGemini on various benchmarks. AlignGemini’s final decision is obtained by applying an OR rule on the fake predictions of the expert branch and the VLM branch: an image is classified as real only if both branches predict it as real. The visualizations show that the two branches provide complementary signals, with the expert model focusing more on pixel-level artifacts and the VLM emphasizing semantic inconsistencies, leading to more robust and generalizable discrimination.

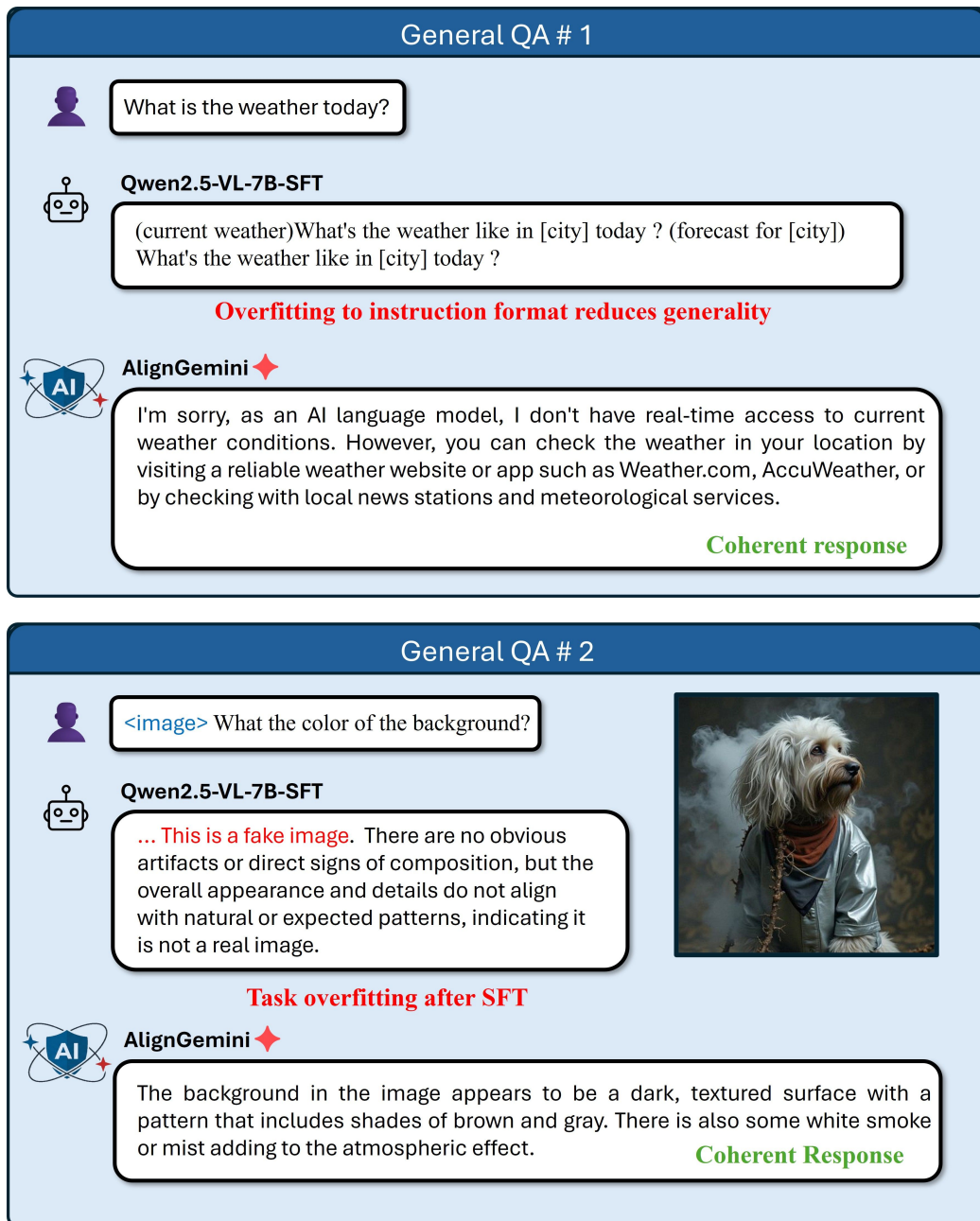


Figure 14. Examples of general multimodal conversations. It indicates that the general capabilities of AlignGemini are largely preserved after adaptation for AIGI detection.

Ground Truth : AI-Generated Image # Pixel-artifact

 <image> Is this image authentic or AI-generated?

 **Align Gemini (◆ OR ◆)**

This is an AI-generated image. ✓

◆ **Expert output**

AI-generated ✓

◆ **VLM output**

<rationale>
 The image shows natural lighting, realistic textures of the bench and dog fur, and a natural outdoor setting with vegetation. There are no telltale signs of AI generation such as inconsistencies in lighting, unusual proportions, or lack of imperfections typical in AI images. The scene is detailed but not overly stylized, which aligns with real-world photography.
 </rationale>
 <answer>
 This is an authentic image.
 </answer>" ✗



Generated Image in AIGI-Now

Ground Truth : AI-Generate Image # Semantically-implausible

 <image> Is this image authentic or AI-generated?

 **Align Gemini (◆ OR ◆)**

This is an AI-generated image. ✓

◆ **Expert output**

Authentic ✗

◆ **VLM output**

<rationale>
 The image displays a highly detailed and symmetrical composition with a level of realism and lighting that goes beyond typical natural variability. The perfect alignment and the flawless texture of the fur and fabric do not align with real-world imperfections. Additionally, the combination of a dog, a cat, and another dog in such a serene and harmonious pose is highly unlikely in reality due to the different temperaments and sizes of these animals.
 </rationale>
 <answer>
 This is an AI-generated image.
 </answer>" ✓



Generated Image in AIGI-Now

Figure 15. Qualitative examples of AlignGemini’s predictions on AI-generated images from the AIGI-Now benchmark.

20

Ground Truth : AI-Generated Image

 `<image>` Is this image authentic or AI-generated?

 **AlignGemini (◆ OR ◆)**

This is an AI-generated image. ✔

◆ **Expert output**

AI-generated ✔

◆ **VLM output**

`<rationale>`
 The image displays natural raindrops on the panda's fur with consistent lighting and realistic water droplet shapes. The fur texture is detailed and varies naturally, with no smudging or repeating patterns typical of AI generation. The background shows depth of field and atmospheric haze consistent with a rainy forest environment. The panda's posture and anatomy are anatomically correct, and the bamboo leaves in the foreground are sharp and naturally lit. No digital artifacts, warped features, or unnatural blending are present. These elements collectively support authenticity.
`</rationale>`
`<answer>` This is an authentic image.`</answer>` ✘



Generated Image in Chameleon

Ground Truth : AI-Generate Image

 `<image>` Is this image authentic or AI-generated?

 **AlignGemini (◆ OR ◆)**

This is an AI-generated image. ✔

◆ **Expert output**

Authentic ✘

◆ **VLM output**

`<rationale>`
 The image depicts a wolf with human-like eyes and a highly stylized, symmetrical facial structure, wearing a red hood that appears to be part of a garment. The fur texture is unnaturally smooth and uniform, with perfect lighting and sharp details that lack natural imperfections. The background is softly blurred in a way typical of AI rendering. Most critically, the combination of a realistic animal face with human-like expression and clothing is semantically implausible in a real photograph, indicating digital synthesis.
`</rationale>`
`<answer>`This is an AI-generated image.`</answer>` ✔



Generated Image in Chameleon

Figure 16. Qualitative examples of AlignGemini’s predictions on images from the Chameleon benchmark.

21

Ground Truth : Authentic Image

 <image> Is this image authentic or AI-generated?

 **AlignGemini** (◆ OR ◆)

This is an **Authentic** image. ✓

◆ **Expert output**

Authentic ✓

◆ **VLM output**

<rationale>

The image features two individuals in formal attire, seated in a room with ornate golden decor, which is consistent with high-profile meetings. However, the level of detail and the natural interaction between the figures, including the subtle shadows and lighting, align more closely with human photography rather than the uniformity typically seen in AI-generated images. Additionally, the presence of a real-world setting with specific historical or cultural elements makes it less likely for this to be AI-generated.

</rationale>

<answer>This is an **authentic** image.</answer> ✓



Authentic Image in Bfree-Online

Ground Truth : AI-Generate Image

 <image> Is this image authentic or AI-generated?

 **AlignGemini** (◆ OR ◆)

This is an **AI-generated** image. ✓

◆ **Expert output**

Authentic ✗

◆ **VLM output**

<rationale>

The image features a person in an orange jumpsuit, which is not typical attire for any real-life scenario involving Donald Trump. The setting and context appear highly staged, with a level of detail and uniformity that is not characteristic of real-world photography. Additionally, the presence of multiple individuals in similar attire and the specific action being performed (sweeping) is not a common or realistic depiction of any public figure's activities.

</rationale>

<answer>This is an **AI-generated** image.</answer> ✓



Generated Image in Bfree-Online

Figure 17. Qualitative examples of AlignGemini’s predictions on images from the BFree-Online benchmark.

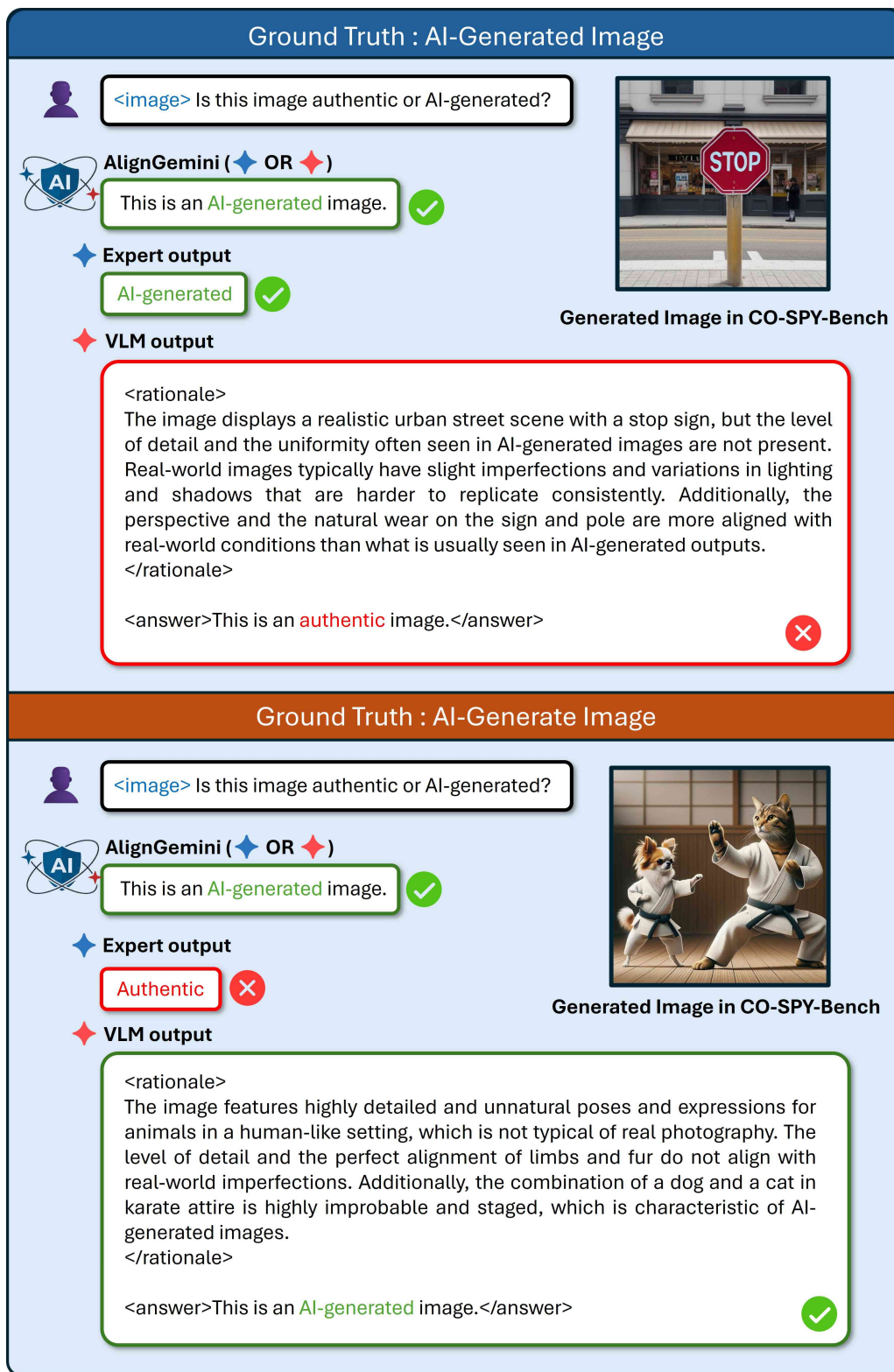


Figure 18. Qualitative examples of AlignGemini’s predictions on images from the CO-SPY-Bench (in-the-wild) benchmark.

Ground Truth : AI-Generated Image

 `<image>` Is this image authentic or AI-generated?

 **Align Gemini** (◆ OR ◆)

This is an AI-generated image. ✔

◆ **Expert output**

AI-generated ✔

◆ **VLM output**

`<rationale>`
 The image displays natural elements like a waterfall and lush vegetation with realistic lighting and textures. However, the vividness and uniformity of the colors, along with the absence of imperfections or anomalies typical in AI-generated images, suggest it could be real. Yet, the slight over-saturation and perfect symmetry might hint at post-processing, which is common in high-quality photography but not definitive proof.
`</rationale>`

`<answer>`This is an authentic image.`</answer>` ✘



Generated Image in WildRF

Ground Truth : AI-Generate Image

 `<image>` Is this image authentic or AI-generated?

 **Align Gemini** (◆ OR ◆)

This is an AI-generated image. ✔

◆ **Expert output**

Authentic ✘

◆ **VLM output**

`<rationale>`
 The image features an astronaut in a stylized, almost surreal environment with an unusual blend of realistic and fantastical elements. The lighting and color saturation are highly uniform and lack the imperfections typically seen in real photographs. Additionally, the astronaut's form appears slightly distorted, which is characteristic of AI-generated images. Real images usually have more varied textures and less perfect symmetry.
`</rationale>`

`<answer>`This is an AI-generated image.`</answer>` ✔



Generated Image in WildRF

Figure 19. Qualitative examples of AlignGemini’s predictions on images from the WildRF benchmark.

24

Ground Truth : AI-Generated Image

 <image> Is this image authentic or AI-generated?

 **AlignGemini** (◆ OR ◆)

This is an AI-generated image. ✓

◆ **Expert output**

AI-generated ✓

◆ **VLM output**

<rationale>

The image displays natural lighting, realistic color gradients in the sky, and detailed textures in the landscape which are typical of high-resolution photographs taken by skilled photographers. AI-generated images often lack the subtle imperfections, varied lighting, and complex interplay of elements seen here. The absence of any anomalies that are commonly found in AI outputs further supports its authenticity.

</rationale>

<answer>This is an authentic image.</answer>



Generated Image in AIGI-Bench

Ground Truth : AI-Generate Image

 <image> Is this image authentic or AI-generated?

 **AlignGemini** (◆ OR ◆)

This is an AI-generated image. ✓

◆ **Expert output**

Authentic ✗

◆ **VLM output**

<rationale>

The image features highly detailed and futuristic elements, including a sleek, modern car with a design not currently in production, advanced architecture with clean lines and a lack of imperfections, and a level of lighting and reflections that are beyond typical real-world photography capabilities. The presence of a watermark indicating AI generation further supports this conclusion.

</rationale>

<answer>This is an AI-generated image.</answer>



Generated Image in AIGI-Bench

Figure 20. Qualitative examples of AlignGemini’s predictions on images from the AIGI-Bench benchmark.